SCIENCE CHINA
Physics, Mechanics & Astronomy

• Invited Review •

February 2026 Vol. 69 No. 2: 224201
https://doi.org/10.1007/s11433-025-2815-1

Organic micro-nanophotonics: Materials, devices and integrated circuits

Xinhuan Xu[1], Hongrui Liu[2], Jialing Jian[3,4], Zequn Chen[3,4], Yiheng Tang[3,4], Wenpeng Ye[5], Yanhua Gao[5], Zhenhua Gao[2*], Lan Li[3,4*], Wenchao Zhao[6*], Kang Wang[1*], Xiaoqin Shen[7*], Xuedong Wang[8*], Wen-Yong Lai[5*], Yuchen Wu[9*], Jiannian Yao[1,10], and Yongli Yan[1*]

[1] *CAS Key Laboratory of Photochemistry, Institute of Chemistry, Chinese Academy of Sciences, Beijing 100190, China*
[2] *School of Materials Science & Engineering, Qilu University of Technology (Shandong Academy of Sciences), Jinan 250353, China*
[3] *Zhejiang Key Laboratory of 3D Micro/Nano Fabrication and Characterization, School of Engineering, Westlake University, Hangzhou 310030, China*
[4] *Institute of Advanced Technology, Westlake Institute for Advanced Study, Hangzhou 310024, China*
[5] *State Key Laboratory of Flexible Electronics (LoFE), Institute of Advanced Materials (IAM), School of Chemistry and Life Science, Nanjing University of Posts and Telecommunications, Nanjing 210023, China*
[6] *College of Materials Science and Engineering, Nanjing Forestry University, Nanjing 210000, China*
[7] *School of Physical Science and Technology, ShanghaiTech University, Shanghai 201210, China*
[8] *Institute of Functional Nano & Soft Materials (FUNSOM), Soochow University, Suzhou 215123, China*
[9] *CAS Key Laboratory of Bio-inspired Materials and Interfacial Science, Technical Institute of Physics and Chemistry, Chinese Academy of Sciences, Beijing 100190, China*
[10] *Institute of Molecular Engineering Plus, College of Chemistry, Fuzhou University, Fuzhou 350108, China*

Received June 4, 2025; accepted September 22, 2025; published online January 4, 2026

Organic micro-nanophotonics is an emerging interdisciplinary field that integrates photonics, nanoscience, and materials chemistry to explore light-matter interactions at the nanoscale. Compared with inorganic counterparts, organic materials offer distinct advantages such as high photoluminescence efficiency, tunable optical properties, and facile processability, which enable flexible and multifunctional nanophotonic applications. This review summarizes recent advances in organic nanophotonic materials and their applications in integrated photonic devices. First, we highlight the unique photophysical characteristics of typical organic materials—including small molecules, conjugated polymers, and hybrid systems—emphasizing their structural versatility and excited-state dynamics. Next, we discuss representative organic photonic devices such as lasers, photodetectors, OLEDs, photovoltaics, modulators, and optical coding systems, focusing on how organic components enhance device functionality. We further review recent progress in the design and fabrication of integrated organic photonic platforms, including patterning techniques, photonic integrated circuits (PICs), and nonlinear photonic systems. Finally, we outline the remaining challenges in the field and provide perspectives on future research directions, particularly in the rational molecular design and structure-property relationship of organic materials. By offering a comprehensive overview, this review aims to promote innovation in the development of tunable, high-performance nanophotonic devices based on organic materials.

organic photonics, organic semiconductors, organic functional devices, integrated optoelectronics

*Corresponding authors (Zhenhua Gao, email: gaozhenhua@qlu.edu.cn; Lan Li, email: lilan@westlake.edu.cn; Wenchao Zhao, email: wenchaozhao@njfu.edu.cn; Kang Wang, email: kangwang@iccas.ac.cn; Xiaoqin Shen, email: shenxq@shanghaitech.edu.cn; Xuedong Wang, email: wangxuedong@suda.edu.cn; Wen-Yong Lai, email: iamwylai@njupt.edu.cn; Yuchen Wu, email: wuyuchen@mail.ipc.ac.cn; Yongli Yan, email: ylyan@iccas.ac.cn)

Citation: X. Xu, H. Liu, J. Jian, Z. Chen, Y. Tang, W. Ye, Y. Gao, Z. Gao, L. Li, W. Zhao, K. Wang, X. Shen, X. Wang, W.-Y. Lai, Y. Wu, J. Yao, and Y. Yan, Organic micro-nanophotonics: Materials, devices and integrated circuits, Sci. China-Phys. Mech. Astron. **69**, 224201 (2026), https://doi.org/10.1007/s11433-025-2815-1

1 Introduction

1.1 Overview of organic photonics

Nanophononics is an interdisciplinary field that merges photonics, nanoscience, and materials chemistry, focusing on light-matter interactions at the nanoscale [1,2]. It encompasses the generation, transmission, modulation, and detection of photons within confined nanostructures. Compared to electrons, photons offer superior information-carrying capacity and faster signal processing, providing significant advantages in modern information technologies. While the advancement of silicon-based electronics has accelerated the development of silicon nanophotonic materials and devices, silicon's indirect and narrow bandgap gives rise to low luminous efficiency, high power consumption, and limited operating frequency. To overcome these challenges, researchers have explored inorganic semiconductors with direct bandgaps, such as ZnO, CdS and GaAs, which show promise in light emission, propagation, detection, amplification, and modulation [3-6]. However, the complex fabrication processes, high production costs, and limited tunability arising from their intrinsic covalent or ionic bonds hinder their broader applicability [7]. As a result, there is growing interest in alternative photonic materials that offer tunable optical properties, facile processing, and cost-effectiveness to expand the library of multifunctional nanophotonic platforms.

1.2 Advantages of organic materials in photonics

Organic materials present a compelling alternative for integrated nanophotonic applications, owing to their outstanding photoluminescence efficiency, tunable optical properties, and fast photon response [8]. π-conjugated small molecules, in particular, can spontaneously self-assemble into ordered nanostructures through weak intermolecular forces such as hydrogen bonding, van der Waals interactions, and π-π stacking [9,10]. These interactions enable the formation of high-quality, low-dimensional photonic structures under mild conditions. By tailoring molecular design, specific non-covalent interactions can be selectively introduced to direct molecular orientation and supramolecular assembly. The resulting micro- and nanostructures exhibit strong optical confinement effects, which are highly sensitive to their spatial dimensions. Such scale-dependent interactions enable enhanced light-matter coupling, exciton diffusion, and emission directionality, thereby unlocking versatile and tunable photonic functionalities [11].

Additionally, organic materials predominantly exhibit localized excited states (Frenkel exciton), characterized by strong dipole transitions and high binding energies (~1 eV), offering superior stability at room temperature compared to Wannier excitons in inorganic semiconductors [12,13]. Organic molecules also support diverse excited-state processes —such as intramolecular charge transfer (ICT) and excimer formation—that allow precise modulation of photon behavior at the wavelength scale [14-16]. In recent years, substantial efforts have been devoted to leveraging these properties for integrated organic photonic circuits by modulating intermolecular interactions and excited-state dynamics [17-19]. Despite these advances, a comprehensive understanding of the promising field, particularly of the structure-property relationship, remains limited and warrants further investigation.

1.3 Scope and structure of the review

Dissimilar to previous review articles that primarily focus on the relationship between self-assembled microcrystal structures, photonic properties, and finite photonic devices, this article provides a comprehensive review of recent progress in organic nanophotonic materials and devices (Figure 1). We start by clarifying the prominent advantages of the typical organic photonic materials including small molecules, conjugated polymers and hybrid materials (Part 2). We then focus on the typical photonic devices that have been developed based on the unique properties of organic nanomaterials to modulate their photonic functionalities, such as organic lasers, organic photodetectors, organic light-emitting diodes (OLEDs), organic photovoltaics (OPVs), modulators, as well as organic coding (Part 3). In subsequent sections, we delve into the rational design and construction of function-oriented organic integrated photonics, aimed at realizing practical nanophotonic applications (Part 4), including several parts of patterning methods, organic photonic integrated circuits (PICs), organic integrated nonlinear photonics. Finally, we put forward the current obstacles and future opportunities in organic nanophotonics. We hope that this review will inspire further innovation in the design and development of tunable nanophotonic devices through exploiting the unique properties of organic nanomaterials.

2 Organic photonic materials

2.1 Organic small molecules

Organic small molecules have revolutionized photonics

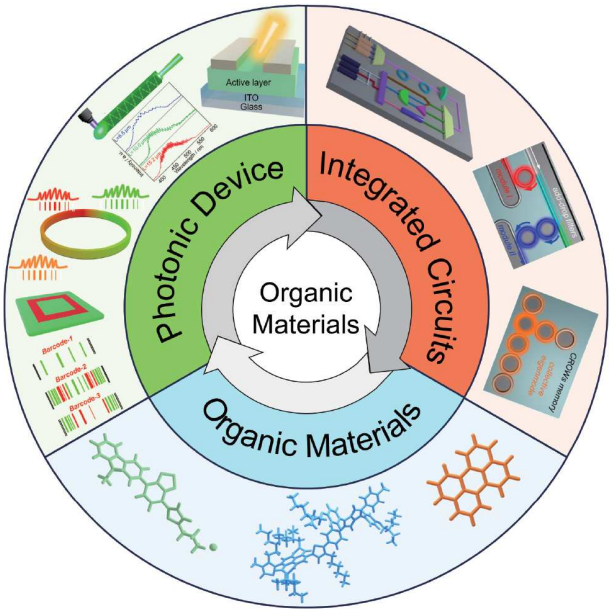

Figure 1 (Color online) Organization of this review. Part 2: organic photonic materials including small molecules, conjugated polymers and hybrid materials. Part 3: typical photonic devices that have been developed based on the unique features of the organic nanomaterials. Reproduced with permission from ref. [11]. Copyright 2016 American Chemical Society. Part 4: construction of function-oriented organic integrated organic photonics toward practical nanophotonic applications. Reproduced with permissions from ref. [17] (Copyright 2013 Wiley-VCH) and ref. [18] (Copyright 2015 American Association for the Advancement of Science (AAAS)).

through their customizable properties, allowing precise manipulation of light-matter interactions at the micro- and nanoscale. Small molecules offer superior purity, well-defined molecular structures, and straightforward synthesis, making them ideal candidates for photonic applications, such as lasing, optical waveguide, and photodetection. This section introduces the foundational principles of organic small molecule photonics and their significance in advancing integrated photonic circuits.

Aromatic compounds, particularly those with large conjugated π-π double bond structures and rigid planar structures, often exhibit significant luminescent properties [20,21]. Their luminescence is generally related to their electronic structure and molecular vibrational states. Upon excitation, electrons transition from the ground state to an excited state, and then release light energy during the process of returning to the ground state, thereby generating luminescence [22]. Aromatic molecules are often used as building blocks for fluorescent materials, with common aromatic molecules serving as the backbones structure of organic molecules as shown in Figure 2(a). Figure 2(a) also displays a portion of planar-extended aromatic molecules, which can be regarded as an extended form of aromatic molecules. These extended systems possess larger conjugation and more stable electronic structures, contributing to more significant electron delocalization throughout the entire molecule [21,23,24].

Substituting functional groups on the aromatic backbone further diversifies the molecular structures, energy levels, and properties. In general, the π-π stacking interaction between molecules gets stronger with increased fused benzene rings [25]. The highest occupied molecular orbital-lowest unoccupied molecular orbital (HOMO-LUMO) energy gap of the molecule may decrease due to the expansion of the electron cloud and the enhancement of π-π stacking interactions. When an electron-donating group is introduced into a molecule, it provides additional electron density to both the HOMO and LUMO orbitals of the molecule, thereby raising both energy levels [26]. However, since the HOMO orbital is closer to the valence electron shell of the molecule, the electron-donating group typically has a more pronounced effect on the HOMO energy level, causing it to rise more significantly [21]. This change results in a decrease in the HOMO-LUMO energy gap of the molecule, which can cause a redshift in the emission wavelength of molecules (Figure 2 (b) and (c)) [27].

Organic cocrystals are single-crystalline materials formed by co-assembly of two or more different organic compounds. The resulting crystal structures differ from their individual components, yielding novel molecular packing and unique electronic and luminescent properties [28-32]. In addition to the basic π-π interactions, cocrystal formation is primarily driven by other non-covalent interactions, such as hydrogen bonding [33,34], halogen bonding [35-37], and charge transfer (CT) interactions [28,38-40] (Figure 2(d)-(f)). In recent years, arene-perfluoroarene (AP) interactions, arising from electron cloud overlap between benzene rings or benzene-like structures of arenes and perfluoroarenes, have also been utilized in the preparation of cocrystals [29,41]. The coexistence of multiple non-covalent interactions allows precise control over cocrystal morphology and properties [34,42,43]. Through reasonable molecular design, solvent selection, temperature control, pressure regulation, and copolymer choice, we can further advance the development and application of cocrystal materials [34,44].

Organic heterostructures have been successfully crafted through the collaborative effort of multiple non-covalent interactions [41,45,46]. It should be highlighted that charge transfer cocrystals exhibit tightly bound donor-acceptor interactions, often resulting in narrower bandgaps compared to individual components [27,39]. These unique energy landscapes enable excellent performance in applications such as emission, waveguiding, and photodetection, with CT cocrystal waveguide emissions reaching up to 950 nm [28,38].

Organic alloys (OAs) are an emerging class of materials inspired by the concept of inorganic alloys, involving continuous substitution in crystalline structures to form A_xB_{1-x}-type solid solutions (Figure 2(g)). This substitution process

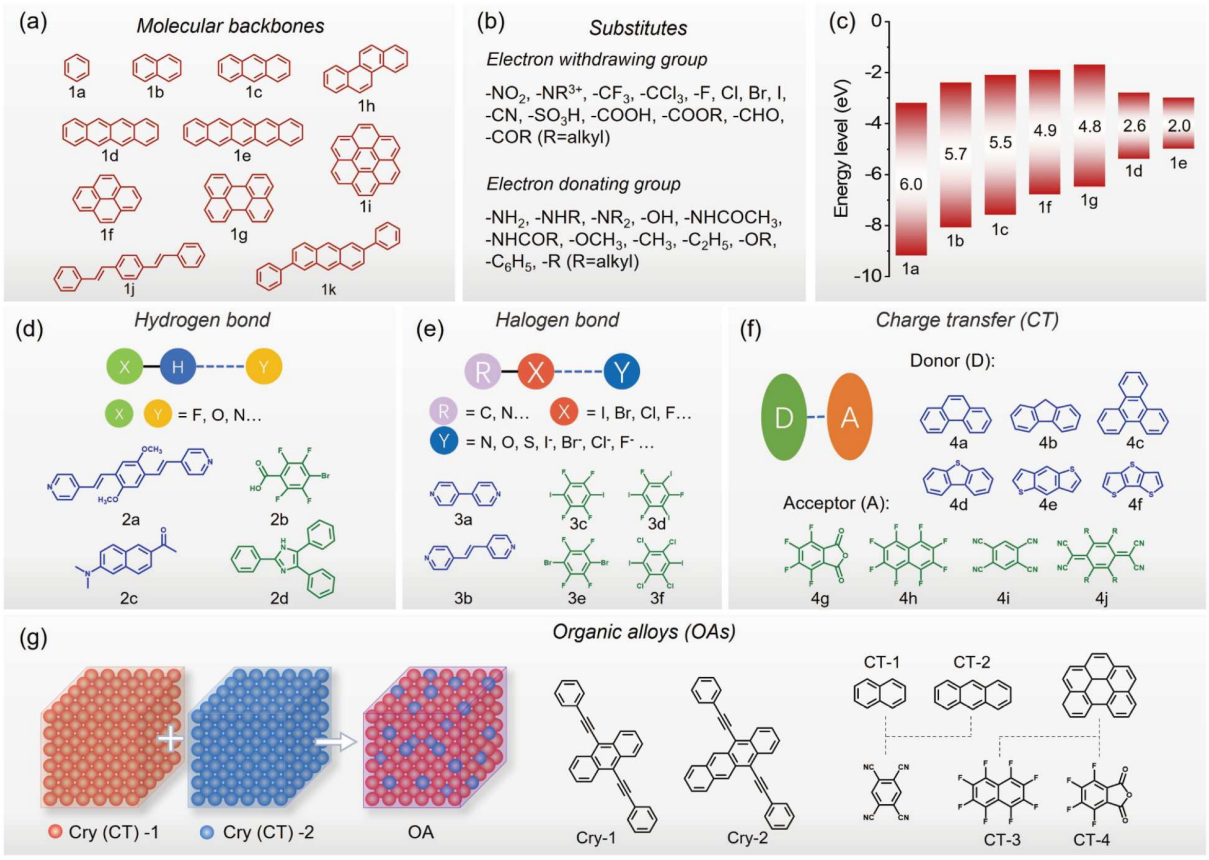

Figure 2 (Color online) (a) Molecular backbones. (b) Electron-withdrawing and electron-donating groups. (c) Energy level of representative π-conjugated molecules displayed in (a). Composition forms and representative molecules of hydrogen bonds (d), halogen bonds (e), charge transfer (f), cocrystals and organic alloys (g).

can vary continuously across a wide range of compositions, thereby endowing the organic alloys with unique physical and chemical properties. First proposed in 1977 by Engler et al. [47] with $TSeF_xTTF_{1-x}TCNQ$ solid solutions, the concept has since expanded across various organic systems. Organic alloys can be derived from single-component polymorphs [48] or from donor-acceptor cocrystal frameworks, where structural compatibility allows for substitution at either the donor or acceptor site [49-55]. As alloy composition changes, properties such as morphology, electronic structure and optical behavior also evolve continuously, enabling precise tuning for targeted applications [51,52,55]. For instance, emission color can be conveniently tuned across the visible spectrum—from blue to red—by adjusting the molar ratio of each component [52]. Furthermore, cocrystalline OAs can facilitate the formation of organic heterostructures with enhanced optical properties [49,50].

2.2 Conjugated polymers

Conjugated polymers (CPs) are a class of macromolecules characterized by alternating single and double bonds along their backbone, allowing for delocalized π-electrons. This π-conjugation endows CPs with unique electronic properties similar to those of semiconductors, while retaining the advantages of lightweight, low-cost, and solution processability. These characteristics make CPs highly promising for applications in fields such as organic field-effect transistors (OFETs), OPVs, and OLEDs [56-58].

While thin-film devices based on conjugated polymers have seen significant performance improvements over the past decades, their inherent limitations—such as poor molecular ordering, high defect densities, and grain boundaries—hinder the study of intrinsic material properties and charge transport mechanisms. In contrast, conjugated polymer micro/nanocrystals offer long-range molecular order, low defect density, and absence of grain boundaries, making them ideal for probing the intrinsic properties, elucidating structure-performance relationships, and constructing high-performance devices. Despite their promise, research in this area remains relatively limited.

This section highlights several representative CP systems to demonstrate the design strategies and device performance, aiming to offer insights for future exploration (Figure 3). The

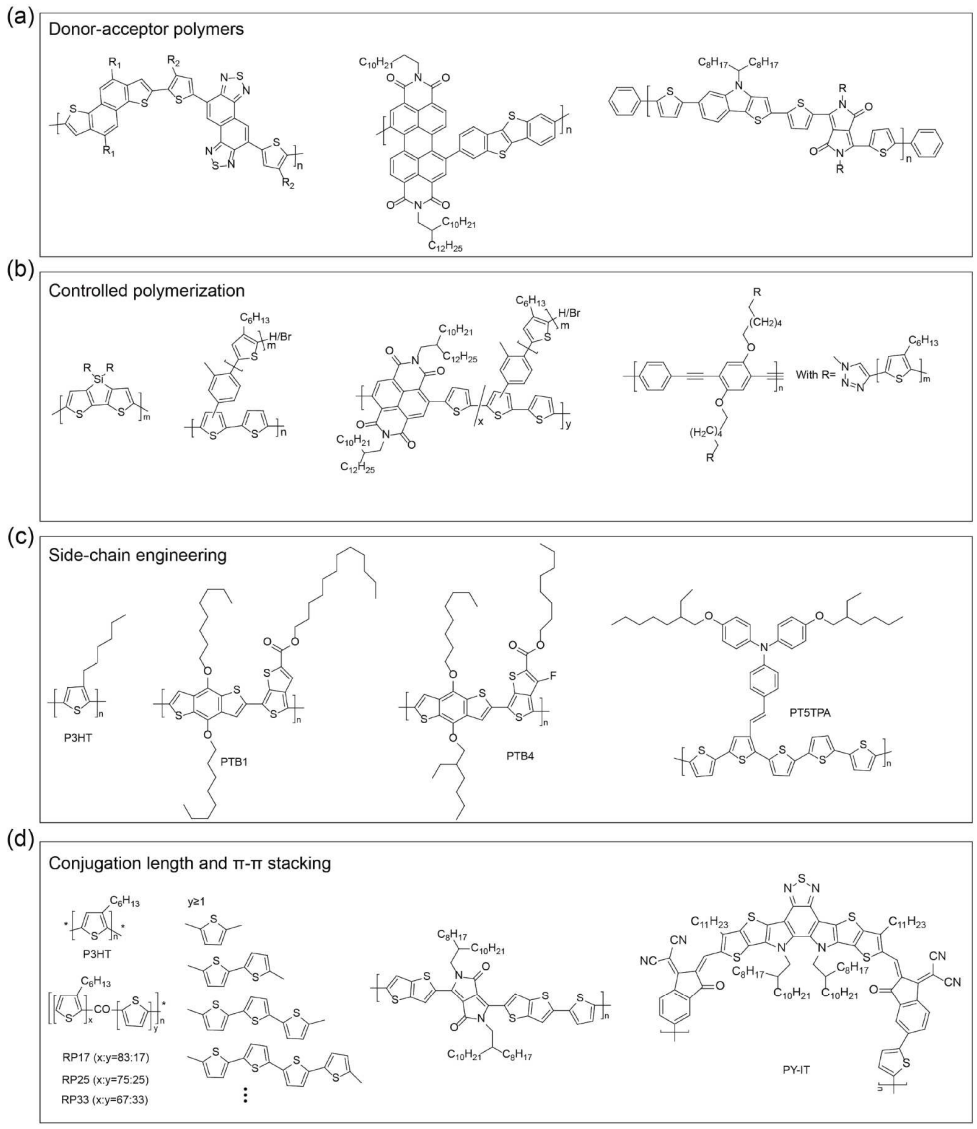

Figure 3 Chemical structures illustrating respresentative molecular design strategies for conjugated polymers: (a) donor-acceptor architectures; (b) controlled polymerization; (c) side-chain engineering; (d) modulation of conjugtion length and π-π stacking.

optoelectronic properties of micro/nano CPs are highly dependent on molecular design, which encompasses the selection of conjugated unit, polymerization techniques, side-chain engineering, conjugation length, and π-π stacking and so on.

2.2.1 Donor-acceptor copolymers

The choice of conjugated building blocks (e.g., thiophene, benzothiadiazole) determines the polymer's electronic and optical properties. Donor-acceptor (D-A) copolymers, which integrate electron-rich donor and electron-deficient acceptor units, enable tunable bandgaps and efficient charge transport. Rational design of electron-withdrawing and electron-donating moieties allows precise tuning of intermolecular interactions, which govern aggregation behavior in solution and packing orientation in the solid state [59].

2.2.2 Controlled polymerization

Controlled polymerization methods, including Stille and Suzuki coupling, afford precise control over molecular weight, chain length, and structural uniformity, thus optimizing material performance for specific applications. These coupling reactions also allow functional groups incorporation at chain ends via initiators or endcappers [60,61]. Two main strategies have been developed: (i) π-complexation between catalysts and growing polymer chains [62,63], and (ii) catalyst-transfer polymerization, inspired by Yokozawa's method for aromatic amides, which enables living polymerization with narrow polydispersity [64].

2.2.3 Side-chain engineering

Side-chain engineering plays a crucial role in tuning solubility, molecular packing, and optoelectronic properties of

CPs. It involves the introduction of flexible chains to enhance solubility, electron-donating/withdrawing substituents to adjust energy levels, and conjugated side chains to extend absorption and improve hole mobility [65,66]. The position and length of alkyl side chains significantly influence the aggregation behavior and crystallinity. For example, regioregular hexyl side-chain in P3HT promotes backbone planarity and ordered packing, resulting in high crystallinity, a narrowed bandgap, and enhanced charge transport. Conversely, regiorandom P3HT exhibits a twisted backbone, reducing conjugation and crystallinity, and causing a blue shift in absorption maxima [67-69].

2.2.4 *π-π stacking*

While π-π stacking is well known to facilitate intermolecular charge transport, its impact on the mechanical properties of conjugated polymers has been less thoroughly explored compared to other dynamic noncovalent interactions. Extending conjugation and enhancing π-π interactions not only improve charge carrier mobility and optical absorption, but also contribute to the mechanical robustness of materials. Park et al. [70] demonstrated that reducing crystallinity while enhancing π-π stacking in thiophene-based random copolymers induces the formation of polymer networks, thereby improving stretchability within fully conjugated semiconducting matrices.

2.2.5 *Conjugated-polymer nanoparticles (CPNPs)*

π-Conjugated polymer nanoparticles offer a versatile platform for emerging applications across optoelectronics, sensing, and biomedicine. Micro/nanofabrication techniques such as electrospinning and nanoimprinting enable the preparation of well-defined nanostructures, including nanowires, nanotubes, and thin films, thereby enhancing material performance. For example, block copolymers such as P3HT-b-poly(2-vinylpyridine) (P3HT-b-P2VP) can be co-assembled with CdSe quantum dots to fabricate nanofibers with aligned quantum dot arrays, demonstrating precise structural control at the nanoscale (Figure 4(a)) [71].

2.2.6 *Composite materials*

Integrating conjugated polymers with functional nanomaterials—such as carbon nanotubes or graphene—can significantly enhance electrical conductivity, mechanical durability, and multifunctionality. Strategies including in situ polymerization, layer-by-layer (LBL) deposition, and surface wrapping have been employed to improve the thermoelectric (TE) performance of such composites [72-74]. For instance, Wang et al. [75] developed a series of composite films for thermoelectric applications, demonstrating the potential of CP-based hybrid systems (Figure 4(b)).

Micro/nano-conjugated polymers exhibited lightweight and flexible features with exceptional electronic properties, bridging the gap between organic and inorganic materials. Micro/nano-conjugated polymers can be designed through diverse strategies and show enormous potential in the fields of electronics, energy and sensing technologies in future.

2.3 Hybrid materials

Hybrid photonic materials represent a fascinating intersection of organic and inorganic chemistry, materials science, and photonics. These materials are designed to manipulate and control light at various scales, offering immense potential for applications in communication, sensing, and display technologies. Among the broad array of hybrid photonic materials, three prominent classes—metal-halide perovskites, metal-organic frameworks (MOFs), and metal-organic complexes—stand out due to their remarkable optical and structural properties. This section explores their distinct features and underlying mechanisms, providing an overview of their role in advancing photonic technologies.

2.3.1 *Metal-halide perovskites: versatile light emitters*

Perovskite materials have emerged as a revolutionary class of photonic materials, capturing significant attention due to their exceptional optical and electronic properties. Named after the mineral perovskite ($CaTiO_3$), these materials are defined by their ABX_3 crystal structure, where A is a

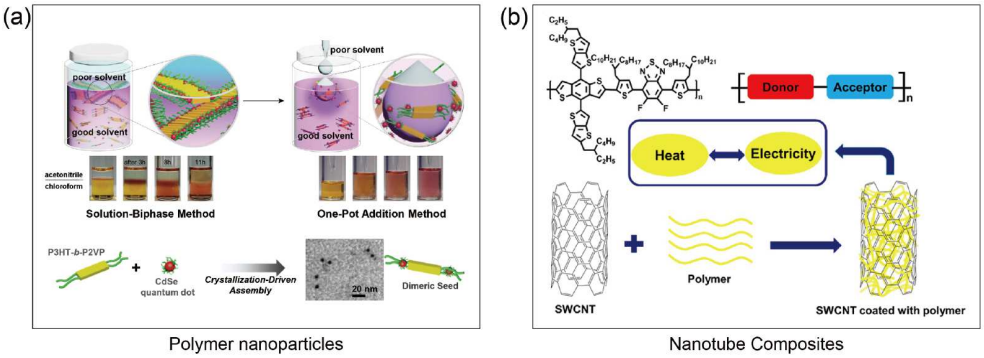

Figure 4 (Color online) Conjugated polymers materials of nanoparticles (a) and composites (b). (a) Reproduced with permission from ref. [71]. Copyright 2016 Wiley-VCH. (b) Reproduced with permission from ref. [75]. Copyright 2018 American Chemical Society (ACS).

monovalent cation (e.g., methylammonium, formamidinium, or cesium), B is a divalent metal cation (e.g., lead or tin), and X is a halide anion (e.g., chloride, bromide, or iodide) [76-79]. Their remarkable attributes include high absorption coefficients, tunable bandgaps, long carrier diffusion lengths, and near-unity photoluminescence quantum yield. One of the most striking features of perovskites lies in their structural flexibility. By altering the composition of A, B, or X, researchers can finely tune their optical properties to achieve desired photonic functionalities. Additionally, their optoelectronic properties can also be adjusted by tailoring their structural dimensionality from 3D to 2D, 1D and 0D. For instance, 2D perovskites consist of alternating organic and inorganic layers, forming a natural quantum well structure. This layered configuration is expressed as $L_2A_{n-1}Pb_nX_{3n+1}$, where L is a bulky organic cation, such as butylammonium, phenylethyl ammonium, BTm, and more (Figure 5(a)). The quantum confinement effect in 2D perovskites results in enhanced exciton binding energies and tunable optical properties. These materials exhibit excellent optoelectronic properties with high photostability, and resistance to environmental degradation compared to 3D perovskites, addressing key stability challenges [80].

Perovskites have made substantial inroads into photonic applications [81]. In lasers, their high optical gain, combined with ease of fabrication, enables the production of low-threshold, tunable lasers [82-85]. In LEDs, their ability to emit light covering the full visible range has pushed the external electricity-to-light quantum efficiency to exceed 32% [86-89]. Furthermore, perovskites exhibit strong nonlinear optical properties, opening avenues for applications in frequency conversion and optical signal processing [90-92]. And the perovskite quantum dots (PQDs) are being explored for applications in high-resolution displays and quantum communication due to their narrow emission linewidths and high quantum yields [93,94]. Notably, the solution processability of perovskites would allow the creation of thin films, nanocrystals, and microstructures under mild conditions, which are essential for waveguiding and integrated photonic devices. Their versatility extends to flexible and lightweight substrates, enabling the development of wearable and portable photonic devices.

Despite these advantages, challenges remain in the widespread adoption of perovskites in photonics. Their intrinsic instability under environmental factors like moisture, heat, and UV radiation poses significant hurdles. Efforts to improve stability through compositional engineering, encapsulation, and the development of hybrid structures are

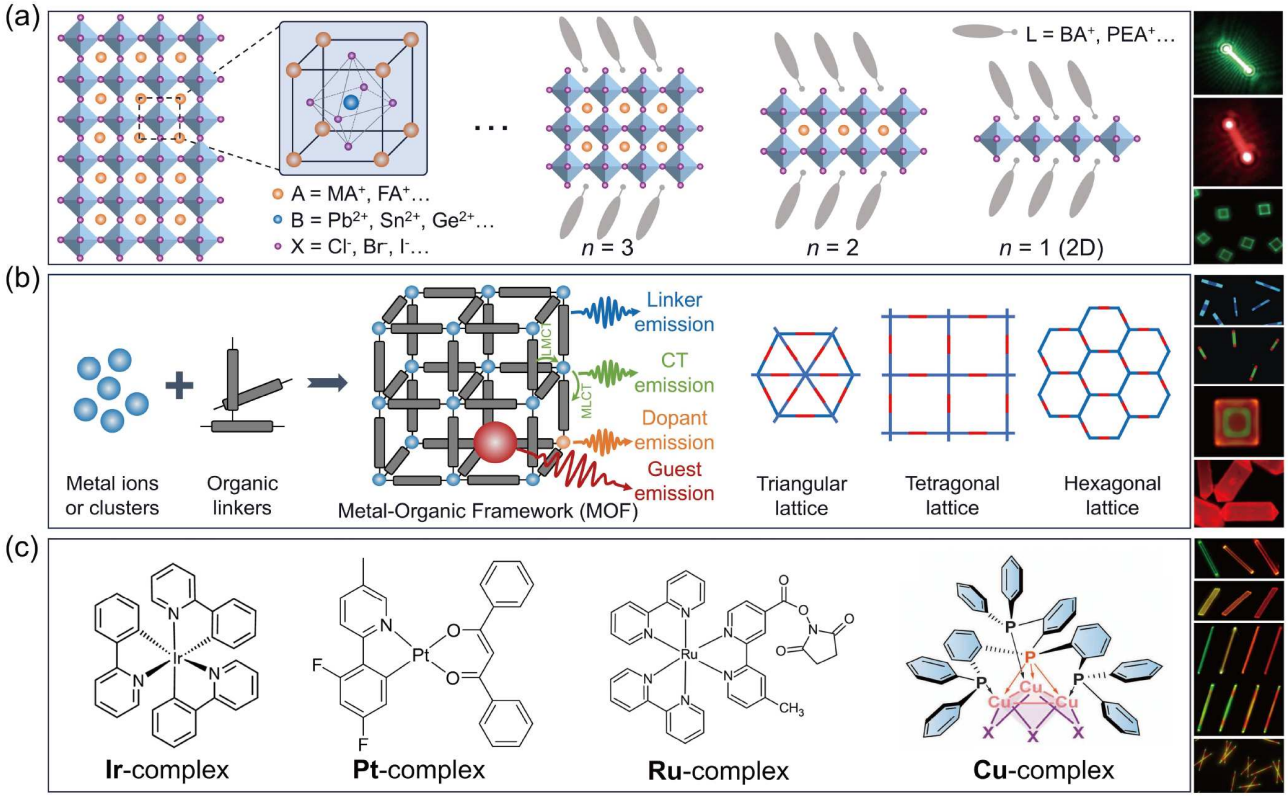

Figure 5 (Color online) Hybrid photonic materials. (a) Organic-inorganic perovskites. Reproduced with permissions from ref. [84] (Copyright 2015 Springer Nature) and ref. [92] (Copyright 2016 Wiley-VCH). (b) Metal-organic frameworks. Reproduced with permissions from refs. [101,102,104] (Copyright 2019, 2021 Wiley-VCH) and ref. [111] (Copyright 2013 Springer Nature). (c) Metal-organic compounds or clusters. Reproduce with permissions from ref. [117] (Copyright 2019 ACS), ref. [118] (Copyright 2024 AAAS [118]) and ref. [121] (Copyright 2018 ACS).

ongoing. Additionally, the presence of lead in many high-performance perovskites raises environmental and health concerns, driving research into lead-free alternatives. In brief, perovskite materials have established themselves as a transformative platform in photonics, offering unmatched optical properties, tunability, and ease of fabrication. Their impact is already evident in a variety of applications, from high-efficiency solar cells to low-threshold lasers. With continued advancements in material stability and environmental safety, perovskites are poised to play a central role in the future of photonic technologies, driving innovations in energy, communication, and sensing.

2.3.2 MOFs: tunable photonic platforms

MOFs are crystalline materials composed of metal nodes connected by organic linkers, forming highly porous and tunable structures. Their unique combination of topological structure modularity, high surface area, and chemical versatility has positioned MOFs as promising candidates for photonic applications [95-98]. One of the defining features of MOFs is their exceptional tunability. By selecting different metal centers and organic linkers, researchers can design MOFs with tailored bandgaps, absorption spectra, and photoluminescence properties based on the processes like ligand-to-metal charge transfer (LMCT), metal-to-ligand charge transfer (MLCT), intra-ligand transitions, and guest emission (Figure 5(b)). For example, incorporating lanthanide ions into MOFs yields materials with sharp emission lines and long luminescence lifetimes [99,100]. This flexibility allows MOFs to operate across a wide range of the electromagnetic spectrum, from ultraviolet to visible and near-infrared regions. Additionally, their ability to exhibit strong luminescence makes them attractive for light-emitting devices, signal processing, sensors, imaging, and anti-counterfeiting applications. For instance, MOFs can be assembled into low-dimensional heterojunctions for signal processing and information encryption [101-104]. Furthermore, their high porosity and large surface area enable the incorporation of guest molecules, further enhancing or modifying their optical properties. MOFs are also valued for their nonlinear optical properties, such as second-harmonic generation and two-photon absorption/emission, which are suitable for frequency conversion, optical switching, and laser technology [105-108]. Moreover, the ability of MOFs to host perovskite quantum dots [109,110], dyes [111-114], or other active species within their pores enhances their photonic functionality, enabling hybrid materials with synergistic optical characteristics [115].

Despite their potential, challenges remain in the widespread adoption of MOFs in photonics. Issues such as limited thermal and mechanical stability, as well as scalability of production, need to be addressed. Ongoing research is focused on improving the robustness of MOFs through structural modifications and developing cost-effective synthesis methods. With continued advancements in material design and processing, MOFs are poised to play a significant role in shaping the future of photonic technologies.

2.3.3 MOCs: dynamic photonic sources

Metal-organic complexes (MOCs) are coordination compounds consisting of metal ions bonded to organic ligands (Figure 5(c)) [116]. These materials are known for their tunable photophysical properties, such as phosphorescence, fluorescence, and charge transfer, which are governed by the nature of the metal center and the surrounding ligands. The ability to control these processes by varying the metal-ligand coordination environment enables precise tuning of their optical properties. These mechanisms allow MOCs to display vibrant emission across the visible and near-infrared regions [117-119], making them suitable for light-emitting diodes (LEDs) providing high brightness and color purity. In addition, MOC can self-assemble into well-defined micro/nanostructures, which can serve as the optical waveguide for photonic integrated systems [120-122]. MOCs are also valuable in sensing applications, where their optical properties can change in response to environmental stimuli such as pH, temperature, or the presence of specific analytes [123-125]. For instance, the luminescence of certain MOCs can be quenched or enhanced upon binding to target molecules, enabling highly sensitive and selective detection. This feature is particularly useful in chemical and biological sensing, where rapid and accurate detection is crucial. Another area where MOCs excel is in nonlinear optics, including strong two-photon absorption and second-harmonic generation capabilities [126-128]. The combination of high optical nonlinearity and structural versatility allows MOCs to be tailored for specific photonic applications, offering advantages over traditional inorganic materials.

Despite their many advantages, the stability and solubility of MOCs often limit their practical applications. Research into robust ligand designs and the incorporation of MOCs into solid-state matrices aims to address these issues, paving the way for their broader use in photonics.

3 Organic photonic devices

3.1 Organic lasers

The realm of organic laser devices has captivated researchers due to its vast potential across multiple domains, including optical communication, sensing, and display technology [129-131]. Organic gain materials, serving as the core of these devices, offer a plethora of advantages that underpin their promise as gain media. Their rich excited-state processes, characterized by substantial stimulated emission cross-sections [8,132], diverse molecular species, and the

capacity to tune emission wavelengths from ultraviolet to infrared [133-135], combined with excellent processability, render them highly attractive [136-138]. In particular, the integration of these materials into micro- and nanoscale architectures has proven effective in enhancing light-matter interactions and enabling compact, high-performance devices.

The journey of organic lasers commenced in 1966 when Sorokin and Schäfer introduced the first organic dye laser [139]. Subsequently, the field witnessed a continuous evolution of organic laser material systems. In 1967, lasing was achieved in dye-doped polymers [140], followed by doped single crystals in 1972 [141], pure anthracene single crystals in 1974 [142], and conjugated polymers in 1992 [143]. These milestones not only marked the expansion of material options but also deepened the understanding of lasing mechanisms within organic matrices. Over time, the miniaturization of optical cavities and the precise control of material morphology at the micro/nanoscale have become central to achieving low thresholds and directional emission.

As shown in Figure 6(a), contemporary research, guided by the Jablonski diagram of organic gain molecule excited states, has identified singlet quasi-four-level transition and stable four-level systems as the preeminent energy level

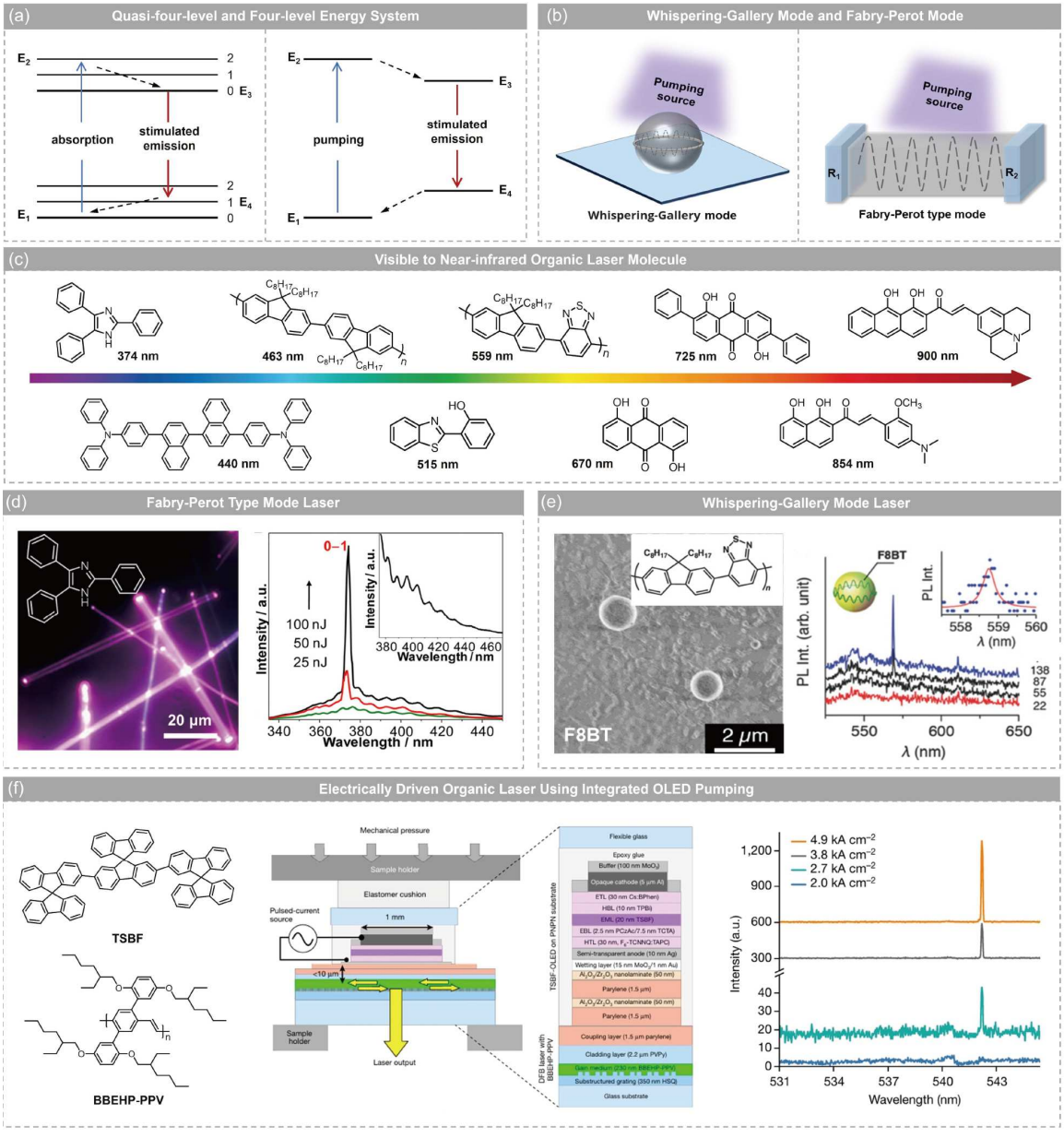

Figure 6 (Color online) (a) Schematic diagram of energy levels. (b) Whispering-Gallery mode and Fabry-Perot mode resonator. (c) Visible to near-infrared organic laser molecule. (d) Single-crystal organic laser of FP resonator. Reproduced with permission from ref. [159]. Copyright 2008 Wiley-VCH. (e) Polymer-organic laser of WGM resonator. Reproduced with permission from ref. [154]. Copyright 2017 Wiley-VCH. (f) Electric organic laser with integrated OLED pump. Reproduced from ref. [162].

architectures [131,144]. These systems provide the necessary framework for population inversion and efficient lasing [145,146]. Importantly, the nanoscale engineering of such energy landscapes—often within confined microcavities—further promotes carrier recombination and mode selectivity, which are essential for laser stability and spectral purity.

Similar to traditional lasers, organic lasers rely on three fundamental components: optical resonant cavities, gain materials, and pumping energy. The optical resonant cavities, which can be categorized into whispering-gallery-mode (WGM) and Fabry-Pérot (FP) types (Figure 6(b)), play a pivotal role in confining and amplifying light [147-150]. The development of these cavities has been instrumental in advancing organic laser technology. The progress in organic gain materials has been remarkable, enabling the emission spectrum of organic lasers to span from 374 nm in the ultraviolet to 900 nm in the near-infrared (Figure 6(c)) [149,151-159]. This broad spectral coverage unlocks diverse application possibilities. By leveraging FP resonant cavities and quasi-four-level gain processes, organic microcrystals have been engineered to fabricate a low-threshold organic laser. In Figure 6(d), the molecular 2,4,5-triphenylimidazole (TPI) self-assembles into nanowires, facilitating strong ultraviolet waveguide and low-threshold ultraviolet lasing at 374 nm (40 nJ/pulse) [159]. Similarly, employing WGM resonant cavities and the molecule F8BT as the gain material, efficient lasing at 558 nm upon 397 nm excitation has been realized (Figure 6(e)) [154].

Despite significant progress, the development of organic lasers faces hurdles, particularly in the pursuit of specialized wavelengths such as electrically pumped and communication band lasers [11,160]. These challenges pertain to material optimization, device fabrication complexity, and energy efficiency enhancement. In a bid to address the challenge of electrically pumped lasers [161]. In Figure 6(f), Samuel et al. [162] devised an integrated-device approach. By integrating molecules TSBF and BBEHP-PPV within organic semiconductors, they achieved an organic indirect electrically pumped laser centered at 542 nm. This breakthrough represents a significant stride in surmounting the obstacles that have long impeded the progress of organic optoelectronics.

In parallel with the development of conventional organic lasers, growing attention has been paid to the generation of circularly polarized light, especially circularly polarized lasing (CPL), owing to its unique advantages in optical communication, quantum information, and chiroptical sensing. Although numerous organic CPL materials have been reported (detailed in recent reviews [163-166]) featuring high photoluminescence quantum yields and dissymmetry factors ($|g_{lum}|$), the realization of circularly polarized organic lasers remains non-trivial, requiring integration of chiral gain materials, high-quality cavities, and low-threshold lasing mechanisms.

Initial advances employed chiral nematic liquid crystals doped with achiral dyes to achieve mirrorless circularly polarized lasing, exploiting selective Bragg reflection. More recent strategies focus on intrinsically chiral organic materials. For instance, chiral π-conjugated polymers co-assembled with dyes enabled circularly polarized random lasing, while small-molecule assemblies with helical microstructures have demonstrated single-mode CPL lasing with high $|g_{lum}|$ values under waveguided feedback [167,168]. Notably, chiral organic crystals with intrinsic gain and spontaneous CPL emission have also been shown to lase under optical pumping, achieving both high efficiency and polarization purity [169,170]. These studies highlight the feasibility and versatility of CPL lasing from all-organic systems, paving the way for next-generation integrated photonic platforms.

3.2 Organic photodetectors

Organic photodetectors (OPDs) are devices that convert light signals into electrical signals by utilizing organic semiconductors (Figure 7(a)), where photon absorption generates excitons that diffuse, dissociate and produce free carriers collected as photocurrent [171]. Compared to conventional inorganic semiconductors, organic materials offer several advantages, including tunable absorption properties, compatibility with flexible substrates and cost-effective fabrication, etc. [172]. In addition to molecular design, recent studies have shown that device performance can be significantly enhanced through the engineering of micro/nanostructures, which can modulate light absorption, exciton diffusion, and charge transport [173]. Driven by materials innovation, micro/nanostructure optimization, and device engineering, OPDs have made significant progress over the past few decades. This section reviews recent developments in OPDs, focusing on polymer-based and small-molecule-based devices.

3.2.1 Polymer-based OPDs

CPs are widely used as active layers in photodetectors due to their flexibility, solution processability, and low cost. However, their intrinsic limitations—such as low sensitivity to weak light—hinder broader application. To address this, Dang et al. [174] developed a new conjugated polymer, PDN, featuring a singlet open-shell ground state (Figure 7(b)). Incorporation of PDN into the active layers remarkably enhanced the photoelectric gain of the devices under low forward bias conditions (Figure 7(c)). Besides, the short diffusion length in polymers limits charge dissociation efficiency. To mitigate this issue, donor-acceptor (D-A) bulk heterostructures have been introduced. The energy offset at the D-A interface promotes exciton dissociation into free charges (Figure 7(d)). For instance, Vella et al. [175] re-

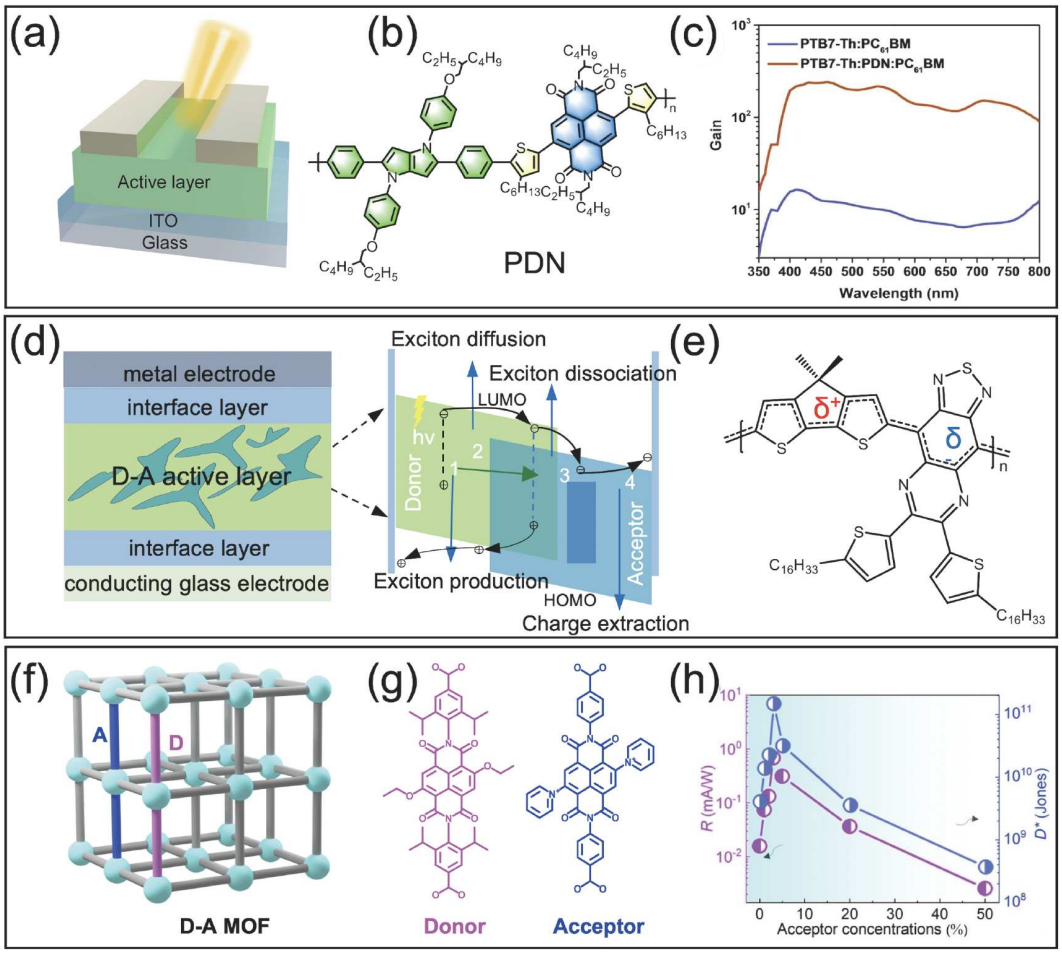

Figure 7 (Color online) (a) Diagram of the device architecture of organic photodetectors. (b) Chemical structures of PDN molecules. (c) Gain of the organic photodetectors with active layers with and without PDN. Reproduced with permission from ref. [174]. Copyright 2023 Wiley-VCH. (d) Cross-sectional view of D-A organic photodetector and exciton diffusion and dissociation mechanism at the donor and acceptor interface. (e) Molecular and electronic structure of the narrow bandgap conjugated polymer. Reproduced with permission from ref. [175]. Copyright 2021 AAAS. (f) Illustration of donor-acceptor MOF structures. (g) Chemical structures of the donor and acceptor linkers. (h) Photoresponsivity of photodetectors based on D-A MOFs. Reproduced with permission from ref. [176]. Copyright 2024 Wiley-VCH.

ported a D-A CP-based photodetector with infrared sensitivity and a detectivity exceeding 2.10×10^9 Jones (Figure 7(e)). Further enhancing charge separation, Xu et al. [176] adopted donor and acceptor naphthalenediimide (NDI) chromophores as linkers in a highly ordered MOF thin film (Figure 7(f) and (g)). The internal donor-acceptor interactions effectively promote charge separation and inhibit carrier recombination, thereby achieving exceptional photoresponse (Figure 7(h)).

3.2.2 *Small molecules-based OPDs*

Although D-A polymer systems effectively promote exciton dissociation, their complex architectures can compromise reproducibility [177]. Small molecules, in contrast, exhibit well-defined molecular structures and regular packing, improving device stability and carrier mobility. For example, Yan et al. [178] synthesized a novel small molecule (SMA, Figure 8(a)) and precisely controlled its crystallization to minimize leakage current and enhance carrier separation, resulting in UV-responsive photodetector with superior self-powered responsivities of 45 mA/W (under 250 nm light) and 70 mA/W (under 300 nm light) (Figure 8(b) and (c)). Unfortunately, typical polycrystalline films often suffer from grain boundaries that hinder charge transport. To address this, Periyanagounder et al. [179] utilized an organic single crystal, $PtBr_2$(5,5′-bis($CF_3CH_2OCH_2$)-2,2′-bpy) (Pt complex), as the active layer (Figure 8(d) and (e)). Its layered crystal structure delivered improved field-effect mobility (Figure 8(f)).

Research has also expanded toward short-wave infrared and polarization-sensitive photodetection. Dong et al. [180] demonstrated a solar-blind ultraviolet photodetector utilizing a wide-bandgap single-crystal organic semiconductor, trans-1,2-bis (5-phenyldithieno [2,3-b:3′,2′-d] thiophen-2-yl) ethene (BPTTE). This device displayed pronounced polarization sensitivity and excellent dichroic ratio (Figure 8(g)-(i)).

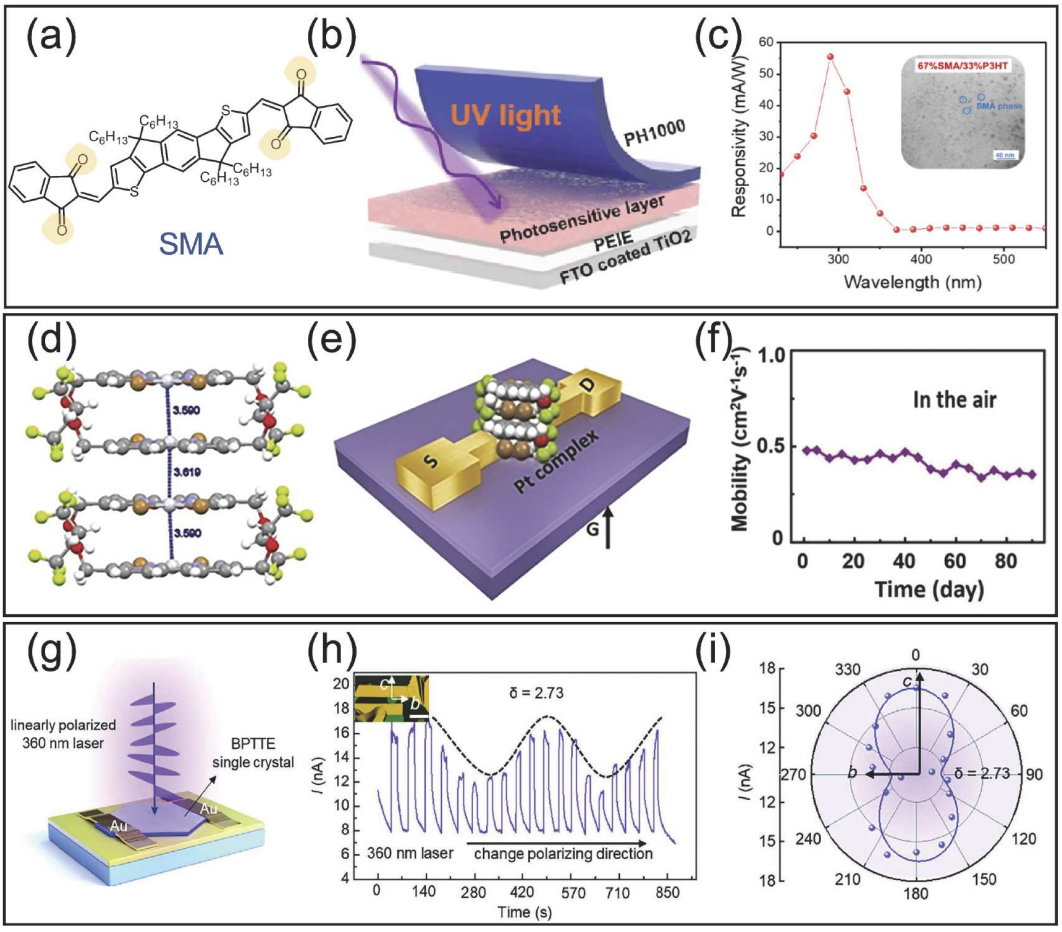

Figure 8 (Color online) (a) Chemical structure of SMA. (b) Device structure of a sandwiched photodetector based on the SMA film. (c) Responsivity of the OPD under different wavelengths of light. Reproduced with permission from ref. [178]. Copyright 2023 ACS. (d) Two units of stacked dimer pairs of the Pt complex crystal. (e) Illustration of the structure of the Pt-complex photodetector device. (f) Time-dependent mobility of the Pt complex under ambient conditions. Reproduced with permission from ref. [179]. Copyright 2019 Wiley-VCH. (g) The schematic diagram of BPTTE single crystal photodetector. (h) Time-resolved polarized optoelectronic response of the BPTTE single-crystal photodetector under linearly polarized light. (i) Polar plot of photocurrent as a function of polarization angle. Reproduced with permission from ref. [180]. Copyright 2024 Wiley-VCH.

In summary, OPDs have achieved significant advancements in sensitivity, spectral selectivity, and structural versatility. Future efforts will likely focus on further improving sensitivity, response speed, and long-term stability, while pushing toward miniaturization and integration into next-generation electronics, particularly for portable and biomedical applications.

3.3 Organic light-emitting diodes

Since the pioneering work by Tang and VanSlyke [181] in 1987 on the first OLED prototype, the field of OLEDs has experienced tremendous evolution in both materials and device engineering. Over the past three decades, the core emissive materials have progressed through three major generations: fluorescent, phosphorescent, and thermally activated delayed fluorescence (TADF) systems (Figure 9(a)) [182]. This evolution has been driven by the need to overcome inherent limitations such as low exciton utilization efficiency, the high cost and limited stability of heavy metal complexes, and issues with device lifetime and color purity. In recent years, additional strategies such as phosphorene/TADF-sensitized fluorescence (TSF) [183-185] and organic radical emitters [186] have further pushed the boundaries of OLED performance, while recent reports of OLED-pumped lasers have opened new avenues for device applications [162].

3.3.1 *Evolution of emissive materials in OLEDs*

Conventional fluorescent materials, which dominated early OLEDs, are inherently limited by a theoretical maximum exciton utilization efficiency of only 25%, as they can only harvest singlet excitons for light emission [187,188]. To circumvent this limitation, phosphorescent emitters based on heavy metal complexes—such as iridium (Ir) and platinum (Pt) compounds—were developed. These materials exploit strong spin-orbit coupling (SOC) to harvest both singlet and triplet excitons, achieving near-unity internal quantum effi-

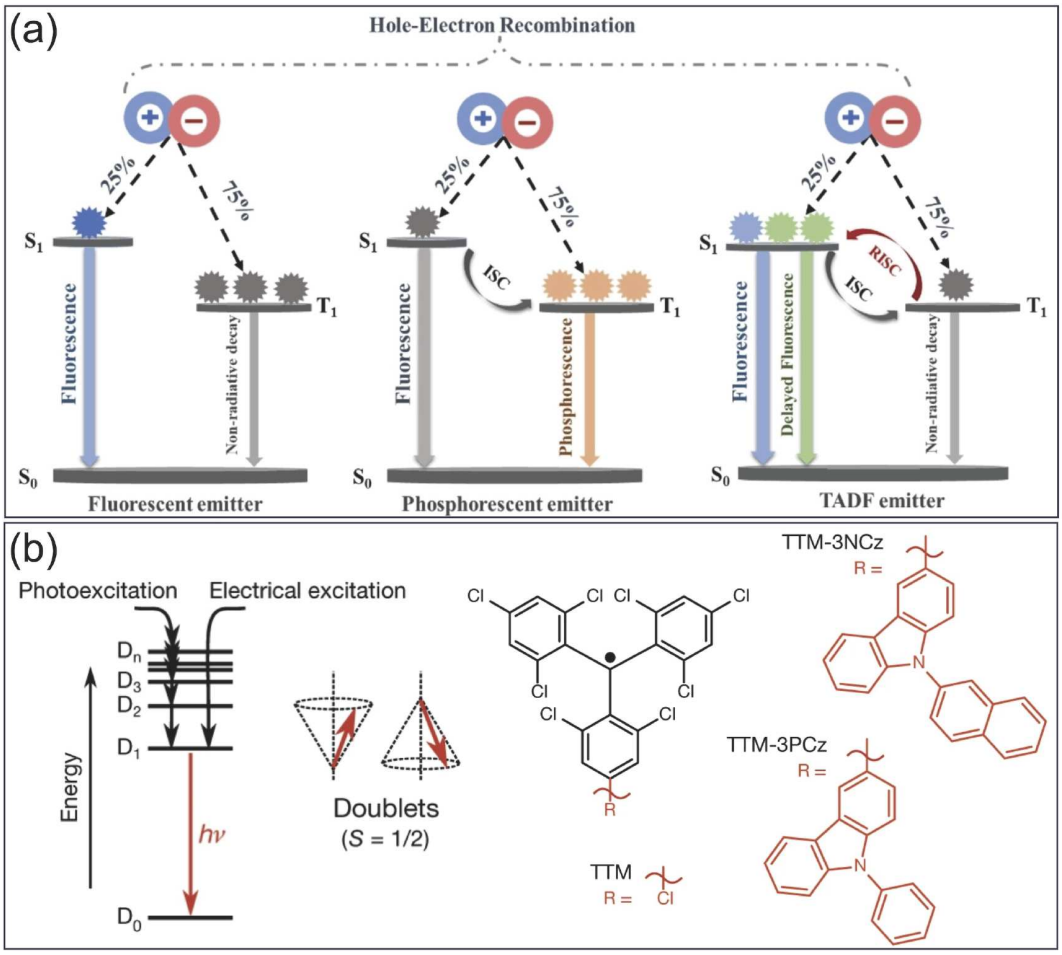

Figure 9 (Color online) (a) Emission mechanism of fluorescent emitter, phosphorescent emitter and TADF emitters. Reproduced with permission from ref. [182]. Copyright 2025 Wiley-VCH. (b) Doublet emission following photo- electrical excitation (left panel) and chemical structures of three representative radicals (right panel). Reproduced with permission from ref. [203]. Copyright 2018 Springer Nature.

ciencies [183,189]. Despite these remarkable efficiencies, the practical deployment of phosphorescent OLEDs is hampered by the high cost of noble metals and issues with stability, particularly for blue emitters, where the high energy of the blue photon often accelerates degradation processes.

A breakthrough in 2012 by Adachi et al. [190] introduced the TADF mechanism, which allows for efficient upconversion of triplet excitons to singlets via reverse intersystem crossing (RISC), thereby enabling 100% exciton utilization without the need for heavy metals. TADF materials have since emerged as a cornerstone for next-generation OLEDs, offering high efficiency, color purity, and cost-effective fabrication [191,192]. The design of TADF molecules relies on the creation of intramolecular charge-transfer (CT) states that minimize the singlet-triplet energy gap (ΔE_{ST}), facilitating RISC. Notably, multi-resonance TADF (MR-TADF) materials, which achieve atomic-level separation of the highest occupied molecular orbital (HOMO) and lowest unoccupied molecular orbital (LUMO) through the incorporation of boron and nitrogen atoms into a rigid framework, have attracted significant attention due to their exceptionally narrow emission bandwidths (FWHM < 30 nm) [193,194]. For instance, Zheng's group [195] at Nanjing University developed TCz-VTCzBN (FWHM = 29 nm, CIE coordinates (0.22, 0.71)), and Duan's team [196] at Tsinghua University designed blue TADF emitters 4CzBN-PhCN, which features an ultralow ΔE_{ST} and a high RISC rate (over 10^6 s^{-1}). These advances in MR-TADF not only satisfy the stringent color purity requirements of ultra-high-definition displays but also extend the operational lifetimes of OLEDs, particularly for blue emission, from tens of hours to the kilohour scale.

3.3.2 TADF-sensitized fluorescence and its impact on device performance

Building on TADF technology, the TSF strategy has emerged as a promising method to combine the high exciton utilization efficiency of TADF with the narrow emission spectra of traditional fluorescent dyes [184,197]. TSF employs a cascade energy transfer process—often mediated by Förster

resonance energy transfer (FRET)—between a TADF sensitizer and a narrowband fluorescent emitter, thereby achieving both high efficiency and excellent color purity [198,199]. For example, Bin and coworkers [200] developed an asymmetric MR-TADF sensitizer, 26tCz-TRZBPI, which resulted in narrowband pure-blue TSF-OLEDs with a maximum external quantum efficiency (EQE) of 24.3%. Very recently, Duan et al. [201] demonstrated a more than twofold increase in the device lifetime and enhanced efficiencies with perdeuterated TADF emitters compared with their protonated counterparts. Further, Su's group [202] at South China University of Technology advanced the TSF approach by designing a series of dual-functional group TSF materials (the DBNDS series), which exhibited an extraordinarily narrow FWHM of only 19 nm, a CIE_y value of 0.77, and EQEs exceeding 34.5%. These breakthroughs in TSF have significantly advanced OLED performance and suggest that TSF could provide a cost-effective alternative to emerging technologies such as Micro-LEDs for next-generation displays.

3.3.3 Organic radical emitters: a new paradigm

Another promising frontier in OLED research is the use of organic radical emitters. Unlike conventional emitters that rely on singlet or triplet excitons, organic radicals emit light through the direct radiative recombination of doublet excitons, theoretically bypassing the 25% efficiency limit and enabling 100% internal quantum efficiency [186,203]. A seminal contribution to this field was made in 2015 by Professor Feng Li's team [186] at Jilin University, who reported the first radical-based OLED utilizing the neutral π-radical TTM-1Cz. This device demonstrated electroluminescence originating from doublet excitons, effectively circumventing the spin-forbidden transitions associated with triplet states in traditional OLEDs. Building upon this foundation, substantial progress has been achieved in enhancing the performance of radical-based OLEDs [203-206]. In 2018, the same research group developed a new radical emitter, TTM-3NCz, which achieved an EQE of up to 27% in the deep-red/near-infrared spectral region (Figure 9(b)) [203]. This advancement set a new benchmark for non-phosphorescent OLEDs and underscored the potential of radical emitters in high-efficiency applications. Despite these advancements, challenges remain, particularly in achieving stable organic radical emitters with a delicate balance between stability and tunable emission properties [204,207].

3.3.4 OLED-pumped lasers: a new milestone

Recent work has also demonstrated the potential of OLEDs to serve as the gain medium for electrically pumped organic lasers, marking a milestone in the field [162,208]. Historically, achieving lasing in OLEDs has been challenging due to issues such as low optical gain, high threshold current densities, and inefficient charge injection [209]. However, pioneering studies have now reported OLED-based devices capable of emitting coherent laser light under electrical pumping. These OLED-pumped lasers leverage advances in high-efficiency TADF and TSF materials to overcome previous limitations. For example, recent work by the Adachi group and collaborators [161] has demonstrated that by optimizing the microcavity structure and engineering the charge transport layers, it is possible to achieve laser action in OLED devices.

Importantly, the realization of lasing in OLEDs critically depends on integrating micro- and nanoscale optical resonators into the device architecture. The use of low-loss, high-Q microcavities enables sufficient optical feedback and spatial confinement necessary for stimulated emission. These nanophotonic strategies significantly enhance light-matter interaction strength. As a result, precise control over cavity dimensions, emitter positioning, and refractive index contrast becomes crucial. The necessity to couple electroluminescent layers with finely engineered micro/nano-cavity structures imposes more stringent requirements on device fabrication. Nevertheless, these advancements not only highlight the feasibility of organic electrically pumped lasers but also open up new possibilities for their application in on-chip optical communications and integrated photonic circuits.

3.4 Organic photovoltaics

OPVs, as an important part of organic electronics, are devices that convert solar energy into electricity. Their fundamental structure comprises electrodes, interfacial layers, and photoactive layers, among which the photoactive layer plays a central role. This layer generally adopts a bulk heterojunction (BHJ) structure, formed by blending a p-type organic semiconductor (donor) with an n-type organic semiconductor (acceptor) [210]. The physical essence of the heterojunction is that the energy barrier formed by the energy level matching at the contact interface of different semiconductor materials directly controls the dissociation efficiency of excitons and the transport performance of free charges.

The operation of OPVs involves a series of complex physical processes, including exciton generation induced by light absorption, exciton diffusion, exciton dissociation at the donor-acceptor interface, free charge migration and recombination, and final charge collection at the electrodes [211]. Among these processes, the efficiencies of exciton dissociation and charge collection are critical to device performance. Unlike inorganic semiconductors, organic materials have a low dielectric constant, leading to the formation of Frenkel excitons with strong Coulombic binding

energies of 0.5-1 eV. These excitons are highly stable at room temperature and dictate the optical properties, energy transfer, and charge generation mechanisms of organic semiconductors. Upon reaching the D-A interface, Frenkel excitons form CT excitons, whose dissociation yields free carriers. Investigating the formation dynamics and dissociation mechanisms of CT excitons remains a central focus in OPV research.

Compared to silicon-based and perovskite solar cells, OPVs suffer from significant energy losses, which are a major bottleneck to efficiency enhancement. Recent advances in non-fullerene acceptor (NFA) materials have offered promising solutions (Figure 10). Unlike traditional fullerene-based systems, NFAs exhibit distinct charge transfer mechanisms [212]. For instance, Yan et al. [213] demonstrated efficient charge separation under low ΔE_{CT} (donor-acceptor energy-level offset) conditions in the P3TEA:SF-PDI$_2$, offering insights into minimizing energy losses. Similarly, Gao et al. [214] showed that optimizing the energy-level alignment between donor and acceptor materials could significantly reduce ΔE_{CT}. They also verified that enhancing the photoluminescence efficiency of narrow-bandgap materials within blends effectively mitigates energy losses. These findings underscore the critical role of designing high-performance materials with low energy loss characteristics in overcoming efficiency limits. However, the intrinsic relationship between the molecular structure of organic photovoltaic materials and key photophysical parameters, such as exciton diffusion coefficient, exciton binding energy, and charge transfer state characteristics, remains inadequately understood. These parameters collectively influence the device's photophysical processes, underscoring the importance of exploring their interplay with molecular structure to optimize device performance.

In recent years, the development of ternary OPV devices has emerged as an effective strategy to regulate exciton and charge dynamics at the physical level. This approach has significantly reduced voltage losses and enhanced device performance. For instance, Zhu et al. [215] used the high-luminescence, high-exciton-delocalization non-fullerene acceptor Z8 into the D18:L8-BO. This successfully modulated exciton dynamics, minimized non-radiative energy losses, and achieved power conversion efficiency (PCE) exceeding 20% in the resulting ternary devices. The ternary strategy optimizes energy alignment to facilitate exciton generation, improves exciton and charge transport efficiency, and suppresses charge recombination. Furthermore, tandem OPV devices represent a promising avenue for surpassing the Shockley-Queisser (S-Q) limit. In recent advancements, their PCE has also exceeded 20% [216].

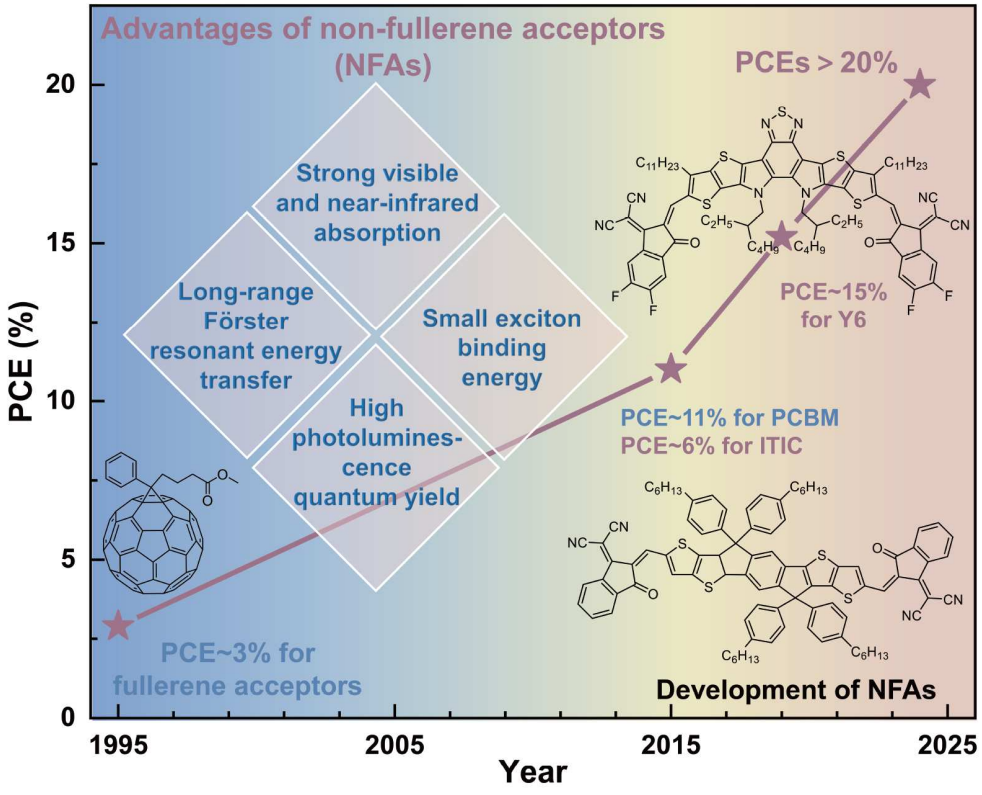

Figure 10 (Color online) Recent advancements in NFAs have significantly enhanced OPV efficiencies. The molecular structures of fullerene and representative NFAs are shown, and the key advantages of NFAs are highlighted, including strong absorption in the visible and near-infrared regions, small exciton binding energy, long-range Förster resonant energy transfer, and high photoluminescence quantum yield.

Active layer morphology optimization is another pivotal aspect of improving OPV performance [217]. Controlling nanoscale phase separation and optimizing carrier transport pathways enhance exciton diffusion and charge migration efficiencies. Looking ahead, continued advancements in OPV materials and device physics, particularly with NFAs, are expected to push PCE beyond the current record of 20% [218], approaching the S-Q limit of 25% for single-junction OPVs. Through a deeper understanding of photoelectric conversion processes and energy loss mechanisms, coupled with innovations in material design and device engineering, OPVs are poised for transformative performance gains.

3.5 Organic modulators

Modulators, as core components in photonic integrated circuits, manipulate the properties of light beams and play a critical role in applications such as high-speed optical communication, quantum computing, optical computing, and artificial intelligence [219-221]. In recent years, there has been extensive research on modulators that incorporate various organic polymers capable of regulating refractive index changes through the electro-optic (EO) effect, with EO polymers [222], liquid crystals (LCs) [223], and organic perovskite materials [224,225], garnering particular interest due to their potential for monolithic integration for compact, high-speed, or low-power consumption modulation.

Due to their substantial EO coefficients, rapid response times, and the ease with which they can be integrated on a large scale, EO polymers have become promising candidates for use in advanced optical modulators. EO polymers comprise a host polymer and highly optically nonlinear organic molecular chromophores that exhibit permanent dipole moments, as shown in Figure 11(a) [226]. The host polymer determines the materials' fundamental refractive index and thermal properties, while the chromophores execute the EO conversion function [223]. To achieve macroscopic second-order nonlinearity, an electric field poling process is performed at high temperatures near the polymer's glass transition temperature (T_g). At this elevated temperature, the chromophores can rotate freely and align under an externally applied electric field, driven by the torque exerted on their molecular dipole moments. Upon significant cooling below T_g, the non-centrosymmetric alignment of the material becomes fixed, enabling second-order nonlinear optical phenomena such as the Pockels effect [227]. Upon applying an electrical signal, the chromophores within the EO polymer undergo electron cloud delocalization. This process will

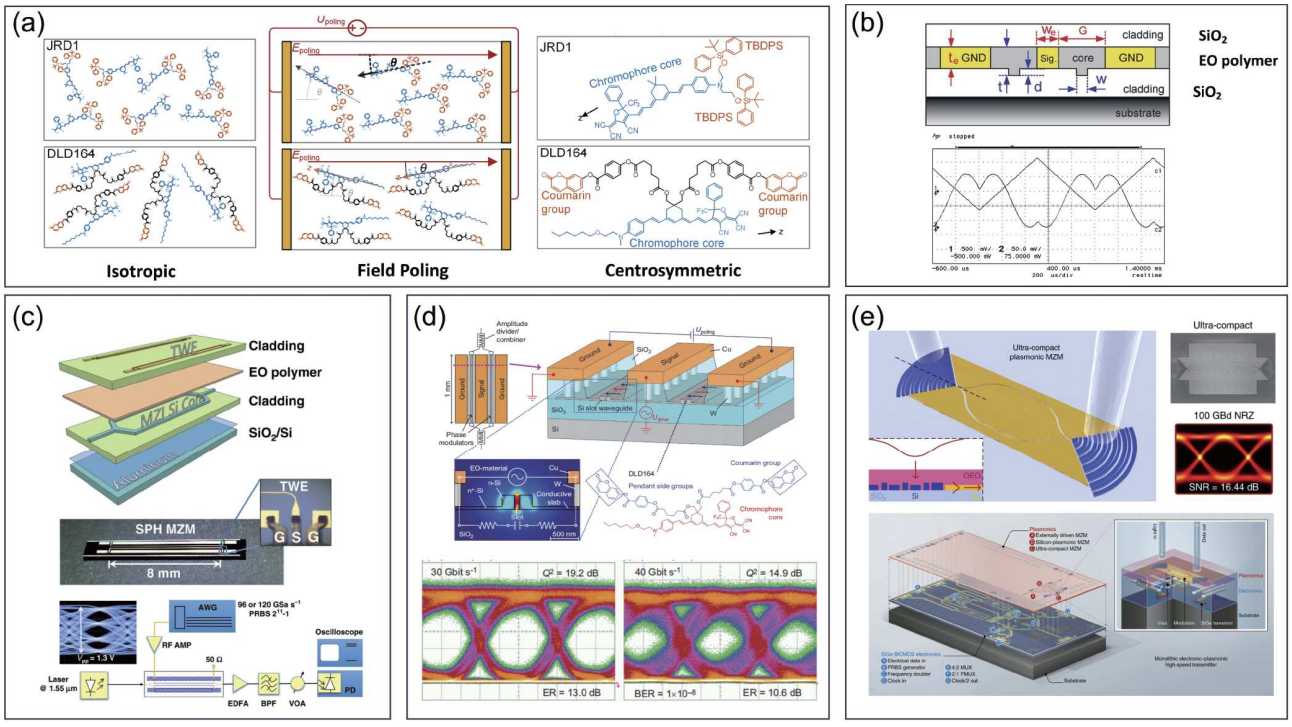

Figure 11 (Color online) Organic electro-optical modulators. (a) Organic electro-optic polymers—from microscopic to macroscopic. Reproduced with permission from ref. [226]. (b) MZI polymer modulator using the conventional Co-Planar Waveguide electrode. Reproduced with permission from ref. [237]. Copyright 2007 IEEE. (c) Silicon-polymer hybrid modulators. Reproduced with permission from ref. [224]. Schematic diagram view of the fabricated devices by layers. Top view photograph of a fabricated Silicon-polymer hybrid modulator chip. Experimental setup for generating PAM4 signals from our fabricated SPH modulator. (d) Silicon-organic hybrid integrated electro-optic modulator. Reproduced with permission from ref. [241]. Copyright 2015 Springer Nature. (e) A monolithic bipolar CMOS electronic-plasmonic organic hybrid integrated high-speed transmitter. Reproduced with permission from ref. [219]. Copyright 2020 Springer Nature.

change the real part of the refractive index, effectively modulating the optical carrier signals [226,228]. EO polymers generally exhibit large EO coefficients (r_{33}), ranging from 300 to 500 pm/V, and have the potential to achieve high EO coefficients of up to 1000 pm/V, based on the theoretical predictions, surpassing those of $LiNbO_3$ films (r_{33}=33 pm/V) by a factor of 10 [229,230]. The Pockels effect in EO polymers originates from the conjugated π-electron system of nonlinear optical molecules. This system features an ultrafast response in electron cloud delocalization, with a phase relaxation time on the femtosecond scale, which enables a theoretical bandwidth exceeding THz when integrated into an EO modulator [228,231,232]. At the same time, the refractive indices of most polymers in the near-infrared are in the 1.5-1.7 range, with similar refractive indices exhibited at microwave frequencies as well. This facilitates the velocity matching between the propagating optical and RF fields when traveling-wave electrodes are used [224,233,234].

EO polymers have attracted extensive research interest, providing crucial technological support for developing high-speed and energy-efficient optical communication systems since 2000 [235,236]. Initially, polymers were used as waveguide materials to realize the functionality of EO modulators, achieving speeds of up to 100 Gbit/s and half-wave voltage-length product of Mach-Zehnder (MZI) modulator 2.2 V_π cm [237,238], as shown in Figure 11(b) [237]. However, due to their relatively low refractive index and poor light confinement capabilities, the resulting devices have excessively long dimensions (3 cm long), restricting their potential for further large-scale integration applications. Subsequently, researchers adopted heterogeneous integration, combining polymers with other dielectric materials such as silicon (Si), TiO_2 and III-V [223,239,240]. This approach improved optical modulation efficiency and reduced device dimensions to the millimeter scale, as shown in Figure 11(c) [224]. However, the interaction between the EO polymer and light remained relatively weak, with insufficient EO overlap, resulting in large power consumption and device sizes. In recent years, Leuthold et al. has proposed two groundbreaking approaches: silicon-organic hybrid (SOH) integrated modulator (Figure 11(d)) [241] and plasmonic-organic hybrid (POH) integrated modulator (Figure 11(e)) [219]. The SOH approach combines silicon slot waveguides with EO polymer cladding, enabling tight confinement of optical and RF modes, thereby enhancing the degree of EO overlap and significantly boosting nonlinear optical effects. This approach has achieved modulators with a length as short as 1 mm, a driving voltage of ⩽ 0.5 V, and sub-millimeter devices with bandwidths exceeding 100 GHz. The low driving voltage (low $U_\pi L$) results in energy efficiency in the femtojoule-per-bit range and, in some cases, even sub-femtojoule-per-bit (attojoule-per-bit) levels (Figure 11(d)) [241-243]. Furthermore, the team developed the POH scheme, which leverages the strong localization capability of plasmonic waveguides to achieve an EO overlap coefficient close to 1 [244]. This reduces device dimensions to the micrometer scale while lowering power consumption to the attojoule level [245].

Plasmonic slot waveguides also serve as electrodes, offering the advantage of low Resistor-Capacitance coefficients, enabling single POH modulator bandwidths of up to 0.5 THz [246], as shown in Figure 11(e). In 2024, the team achieved a 1.6 THz optical module product, highlighting the immense potential of EO polymers in high-speed optical communication [247]. However, the polymer structure remains a limiting factor, with thermal stability being a target for optimization. Although there have been reports of devices operating at 85°C for over 2000 h, further improvements are needed for practical applications [248]. EO polymers often face trade-offs between achieving a high EO coefficient, thermal stability, and material compatibility for device integration. Neat chromophore systems can achieve high r_{33} but lack sufficient thermal stability, while traditional polymer-host systems dilute chromophore density, limiting their performance [249]. Xu et al. [227,230,231] developed a novel cross-linkable binary molecular glass system using two chromophores, HLD1 and HLD2, that can be thermally cross-linked after electric field poling. This work represents a significant step toward practical, high-performance organic EO materials for next-generation optical communication and signal processing devices.

In recent years, solution-processed organic perovskites have also demonstrated similar EO modulation capabilities, offering advantages such as low cost, high photoelectric activity, and straightforward fabrication processes. The EO response of the organic perovskite approaches that of $LiNbO_3$ and highlights the promise of rationally designed organic perovskites for use in efficient EO modulators [250]. However, compared to traditional organic EO materials, the stability and consistency of the processing of perovskites remain key challenges to address.

In addition, silicon photonic devices have achieved remarkable diversification, shifting the focus towards integrating more complex systems on a single chip. In this context, optical phase shifters serve as key components in systems such as switches, polarization controllers, advanced receivers, and optical signal processors. The required response times range from a few microseconds (for switching and tuning) to several milliseconds (for mitigating environmental influences). While the speed requirements are relatively relaxed, compact device size, low driving voltage, and ultra-low power consumption are of paramount importance [251]. LC molecules are highly birefringent, and their orientation can be electrically controlled by external electric fields. LC phase shifters based on Si slot waveguide combine a large overlap of the optical mode field and the liquid crystal

cladding with a small separation and a fully planar configuration of the electrodes [252]. A 30π phase shift with a 1 V drive voltage and 1 mm long phase shifter has been demonstrated in a LC-filled MZI switch [253]. Aside from the above, Jian et al. [254] reported the use of plasmonic waveguides to enhance polymer-stabilized liquid crystals. By electrically controlling the scattering state of the polymer-stabilized liquid crystal, they achieved an extinction ratio of 0.38 dB/μm within a 10-μm-long device, while simultaneously reducing the response time of the liquid crystal device to the microsecond scale. This represents a novel approach to compact optical attenuators for low power consumption.

EO modulators based on organic materials have demonstrated significant potential in a wide range of applications, including telecommunication and data communication, optical interconnects, and RF sensing. To address the growing demands for data processing in fields such as artificial intelligence, quantum communication, and the Internet of Everything, organic materials require further optimization. This includes improving the T_g through compositional adjustments, enhancing EO conversion efficiency, and advancing long-term stability.

3.6 Organic coding

Organic micro/nanoscale photonic barcodes have shown enormous potential in modern data storage and security applications due to their compact size, high information density. Organic materials are favored in construction of the micro/nanoscale photonic barcodes due to their tunable optoelectronics [255]. The following section presents the research advancements in organic photonic barcodes, focusing on encoding strategies including graphical and spectroscopic encoding.

3.6.1 Spectroscopic encoding

Spectral encoding utilizes both the color and intensity of light emitted from the multicolor-emitting materials to serve as the identification code (Figure 12(a)). Due to the isotropic nature of photoluminescence, spectral encoding offers convenient identification without orientation dependence. Luminescent organic molecules with abundant emission spectra make it possible to create a diverse library for spectroscopic encoding. Xiao et al. [256] introduced a method for encoding microspheres composed of intramolecular through-bond energy transfer (TBET) molecules. Three unique boron dipyrromethene derivatives with clearly separated emission bands were chosen to create the encoding cassettes, enabling highly efficient TBET with a single excitation wavelength (Figure 12(b)). These microspheres emitted three discrete fluorescence peaks simultaneously without interference, thus demonstrating potential for multi-channel and high-throughput analysis.

However, the wide photoluminescence (PL) bands of various materials frequently overlap, thus restricting the encoding capacity [257,258]. To address this problem, Zhao's group [259] proposed a barcode design based on whispering-gallery mode (WGM) modulation in dye-doped microdisks (Figure 12(c)), which produces a photoluminescent spectrum featuring a range of sharp peaks due to WGM modulation (Figure 12(d)). These photonic barcodes offer virtually unlimited encoding capacity by varying the size of the microdisks (Figure 12(e)), making them promising for anti-counterfeiting and information security applications [259]. Based on this, Gao's group [260] developed a surface tension-assisted self-assembly approach to fabricate multicolor WGM microrings with tunable spatial components. By modulating the CT strength between electron acceptors and doped donors (Figure 12(f)), full-color microrings were finally prepared, exhibiting distinguishable peaks with size-dependent characteristics, ideal for high-quality photonic barcode applications (Figure 12(g)-(i)).

3.6.2 Graphical encoding

Graphical encoding utilizes visual elements like color, shape, size, or position features to represent information elements about the objects depicted (Figure 13(a)), thereby reducing data volume and enhancing coding capacity. One-dimensional organic heterostructure nanowires are extensively employed in the field of optical encoding due to their capability to integrate diverse electrical and optical properties [103]. Zhao et al. [261] developed an axially tunable one-dimensional organic luminescent heterostructure, where small organic molecules are progressively assembled into multi-block structures with tunable color properties (Figure 13(b) and (c)). This assembly is achieved by precisely controlling host-guest molecular interactions, significantly enhancing graphic coding potential. However, the passivation of pre-fabricated crystals during the epitaxial growth of heterostructures frequently impedes their subsequent self-assembly capabilities. To address this, Gao et al. [262] proposed a directional self-assembly strategy for organic epitaxial heterostructures, which are formed through directional facet identification between different building blocks, thus resulting in spatially resolved emission colors and distinct patterns (Figure 13(d)-(g)).

In contrast to one-dimensional heterostructures, two-dimensional heterostructures can store and transmit information across multiple directions within the plane, thereby further increasing encoding density. Gao et al. [104] developed a controllable synthetic method based on spatial semi-confinement-induced steric hindrance for fabricating lateral Ln-MOF heterostructures with tunable dimensions (Figure 13(h)). By introducing channel-directed guest modulators, the in-plane and out-of-plane growth rates of the Ln-MOF

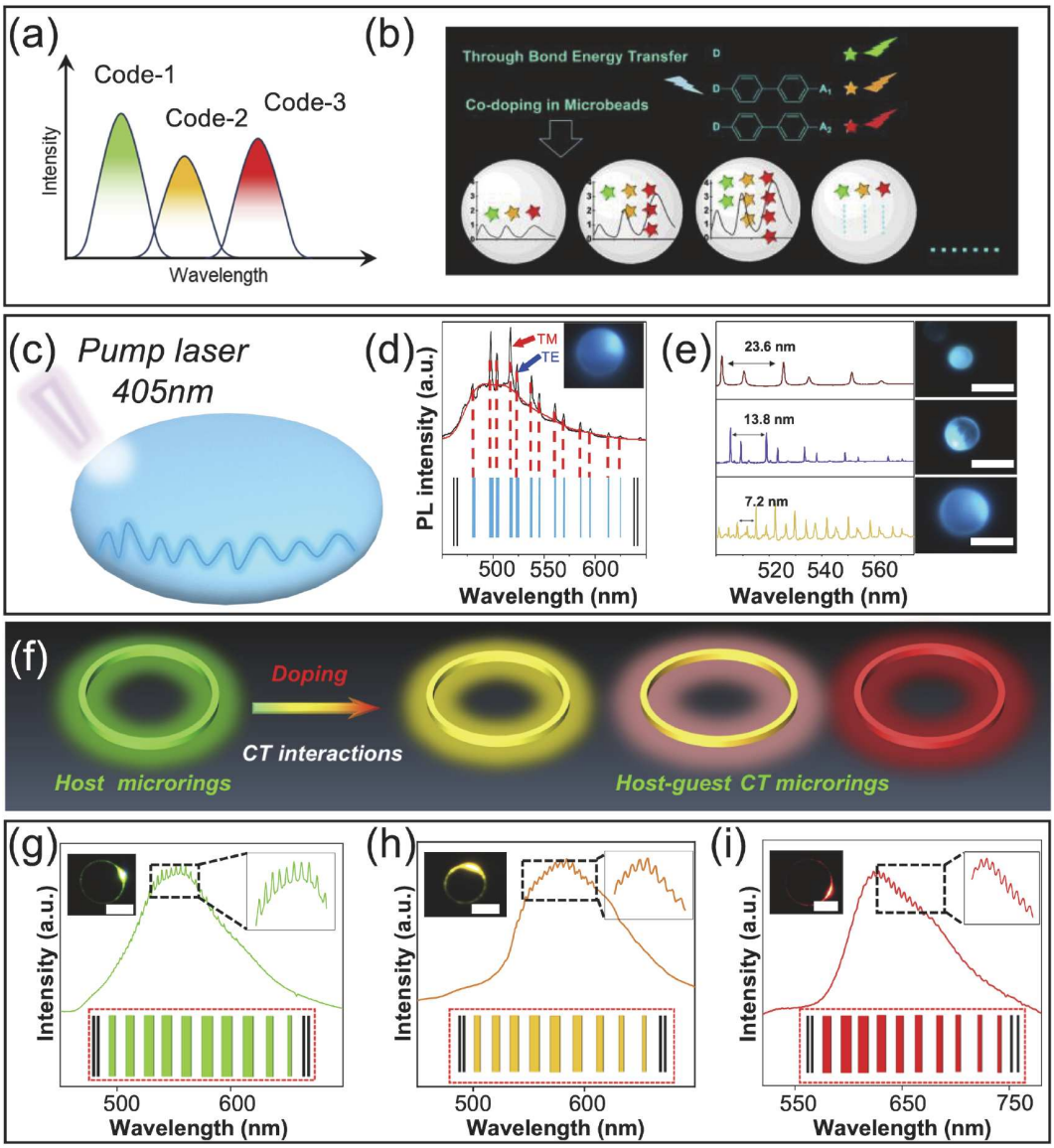

Figure 12 (Color online) (a) Schematic illustration of the spectral coding strategy. (b) Diagrammatic sketch of the energy transfer via bonds (TBET). Reproduced with permission from ref. [256]. Copyright 2014 ACS. (c) Schematic illustration of WGM cavity effects a single microdisk under a 405 nm CW laser excitation. (d) Photoluminescence spectra of typical microdisks, showing the corresponding photon barcodes. (e) WGM modulation observed in three microdisks of varying sizes. Reproduced with permission from ref. [259]. Copyright 2017 Wiley-VCH. (f) Illustration of the generation of polychromatic microrings through modulated CT interactions. (g)-(i) WGM resonance spectra of typical microrings through modulated CT interactions, with corresponding photon barcodes. Reproduced with permission from ref. [260]. Copyright 2023 Wiley-VCH.

crystals can be effectively controlled. Furthermore, benefitting from the isostructural properties of various Ln-MOFs, epitaxial growth of two- or three-segment concentric heterostructures with different emission colors can be achieved, enabling the creation of spatially resolved planar 2D photonic barcodes (Figure 13(i)).

In summary, organic photonic barcodes hold great promise for applications in data storage, secure communication, and anti-counterfeiting. By manipulating light at the molecular level, organic materials enable the construction of customizable and efficient photonic devices. Progress in these areas will be essential for realizing the full potential of organic photonic barcodes in next-generation photonic and optoelectronic integrated technologies.

4 Integrated organic photonics

4.1 Patterning methods

Integrated organic heterostructures combine different optoelectronic functional materials to produce micro- and nanodevices with multiple functions and high performance, such as full-color laser displays, OLEDs and photodetectors. Hierarchical heterostructures have obvious advantages over

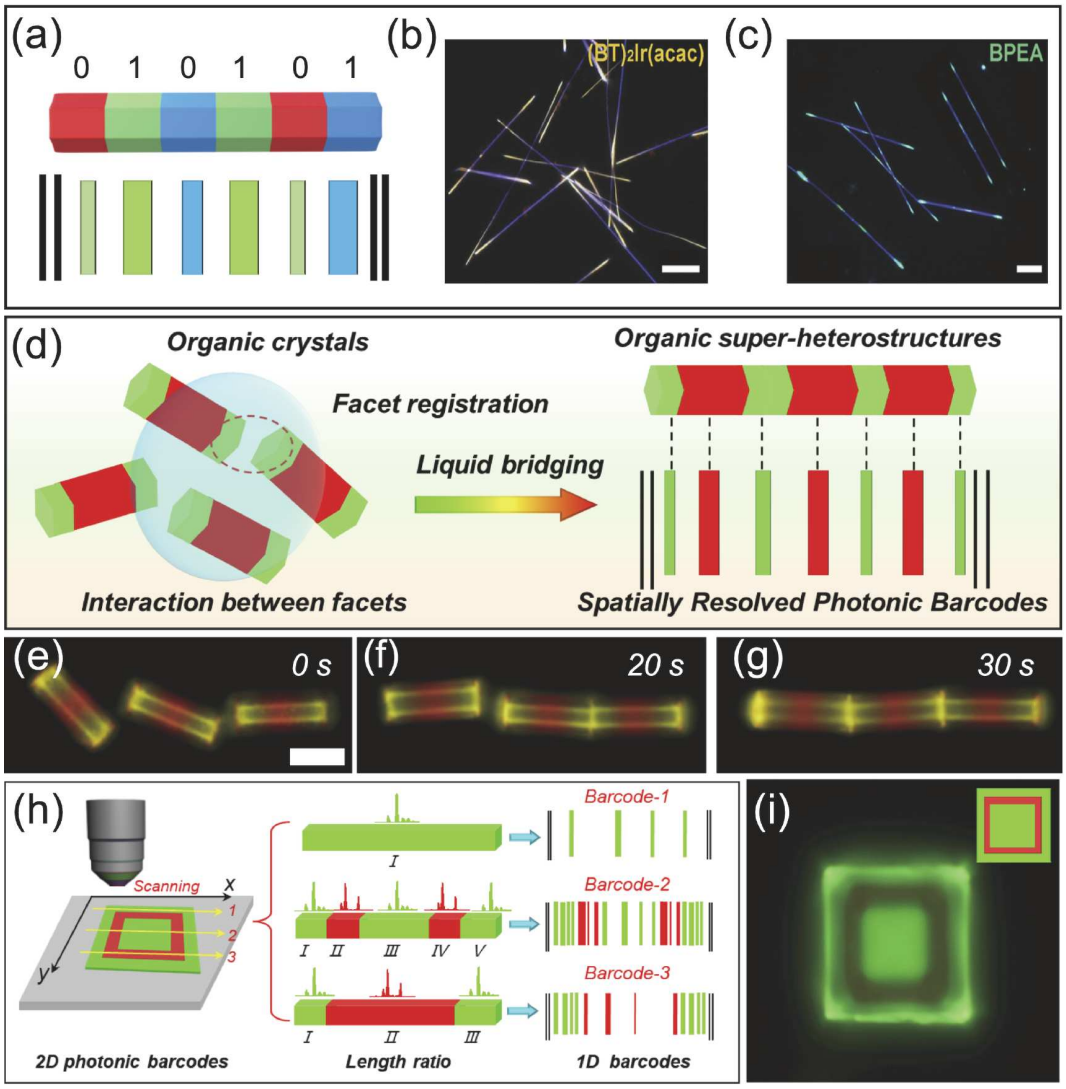

Figure 13 (Color online) (a) Schematic illustration of the graphical encoding strategy. (b) Tri-block (BT)Ir(acac) and (c) multi-block BPEA-doped TPI microtubes. Reproduced with permission from ref. [261]. Copyright 2012 Wiley-VCH. (d) Diagram of the directional self-assembly process for organic heterostructures, enabling the creation of spatially resolved photon barcodes. (e)-(g) PL images of the reorientation process of the three building blocks. Reproduced with permission from ref. [262]. Copyright 2023 ACS. (h) Schematic representation of the encoding strategy based on a three-segment concentric Ln-MOF heterostructure. (i) PL images of the three-segment 2D concentric heterostructures. Reproduced with permission from ref. [104]. Copyright 2021 Wiley-VCH.

single-component optoelectronic functional materials, such as tunable device performance, which can be controlled by adjusting the components, and programmable physical properties, which are induced by designing the geometric structures. However, the fabrication of high quality integrated organic heterostructures remains challenging for the following reasons: (1) solvents used in subsequent operations during multi-solution processing can dissolve and destroy previously formed structures, and (2) different materials and solutions exhibit different assembly and fluid behaviors, respectively. To address these issues, many researchers have worked to pattern hierarchical heterostructures in an efficient and controllable manner, and have developed several viable fabrication techniques. Solution-based methods, such as inkjet printing and self-assembly, enable precise patterning of organic materials with low-cost, scalable processing. Photolithographic techniques, often combined with dry lift-off or mask-based patterning, provide high-resolution control for complex multicolor and lateral heterostructures. Vapor deposition methods, including physical vapor deposition (PVD) and chemical vapor deposition (CVD), are widely used to fabricate vertically stacked heterostructures, ensuring uniformity and material purity. In this section, we present representative work on patterning methods for multicomponent materials. According to the relative spatial location, the integrated organic photonic devices can be classified into lateral and vertical integrated devices (Figure 14).

4.1.1 *Lateral integrated organic photonics*

Thermal evaporation is one of the most commonly used methods for fabricating high-quality, full-color OLEDs, especially for high-performance display devices used in smartphones and TVs. Vacuum deposition offers precision in forming organic emitting layers, ensuring uniform film thickness and high-purity materials. A shadow mask is used to selectively deposit emissive layers (red, green, blue) for different subpixels in the display to create full-color OLEDs. After multi-step deposition, the different organic vaporized material condenses on the substrate, forming a high-purity, uniform organic heterogenous pattern. Because of the usually anisotropic shape of organic molecules and the weak van der Waals interactions between the molecules, the growth of the organics is more challenging than the inorganics, of which the shape is more isotropic and the mutual interaction is much stronger [263]. Nevertheless, vapor deposition can offer exceptional precision and uniformity in the fabrication of RGB OLED displays. Its capability to achieve high material purity and scalability for large-area substrates ensures its suitability for producing high-performance full-color OLED displays. Choi et al. [264] fabricated a full-color OLED display on a large-area MoS_2 backplane, demonstrating a wearable and flexible active-matrix device.

Epitaxial-growth process offers a universal method to organic systems with facile chemical/structural compatibility for fabricating the desired organic heterostructures. Lateral epitaxy is an effective method to fabricate 1D and 2D heterojunction arrays. Wang et al. [265] demonstrated the growth phenomenon of epitaxial-growth process in hierarchical self-assembly and fabricated 1D organic core-shell heterostructures. Wang et al. further optimized the vapor deposition method to fabricate two-dimensional heterojunction arrays. By utilizing the different sublimation points of Pe and PeO, they achieved sequential nucleation and growth, where Pe sublimated first to form seed crystals, followed by the lateral epitaxial growth of PeO at the crystal edges. This process ensured minimal lattice mismatch and clean heterojunction interfaces. The general applicability of the lateral epitaxy strategy for 2D organic lateral heterostructures was successfully validated through the synthesis of Py-DbPy, MePy-Pe, and BGP-PeO heterostructures [265].

Direct photolithographic patterning of organic semiconductors has been demonstrated by exploiting ultraviolet-sensitive photo-cross-linkable additives [266]. In this approach, the OSC films with photo-crosslinkers are processed as conventional photoresists, enabling selective modulation of film solubility in UV exposure regions. Consequently, the soluble regions are eliminated via a solvent washing process. Although this methodology enables the OSC patterns of micron-scale and multi-pattern processing, the realized pattern sizes are insufficient for the implementation of high-density OLEDs. Kim and his collaborators [267] used conventional photolithography in combination with the reactive ion etching dry process to address the issue of well-defined high-resolution pixelation in the display industry. Specially, they present a silicone-engineered anisotropic lithography of the organic light-emitting semiconductor that *in-situ* forms a non-volatile etch-blocking layer during reactive ion etching. This unique feature not only slows the etch rate but also enhances the anisotropy of etch direction, leading to the gain of delicate control in forming ultrahigh-density multicolor

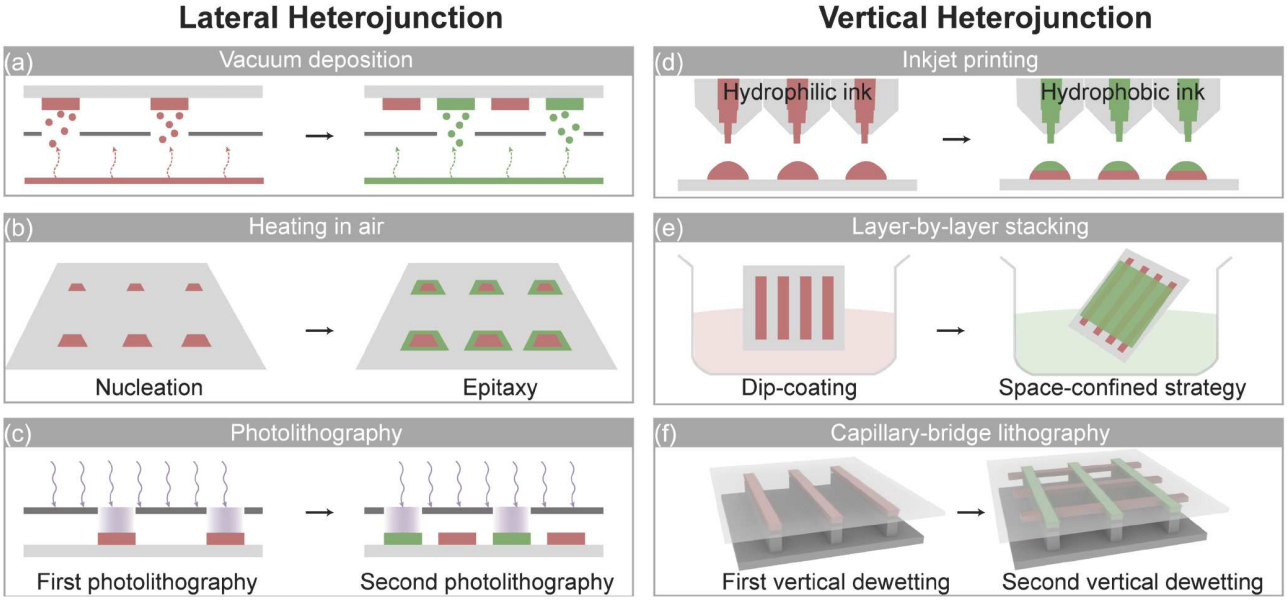

Figure 14 (Color online) Patterning methods of integrated organic photonics. (a)-(c) Schematic illustrations of lateral integrated photonics, including (a) vacuum deposition, (b) lateral epitaxy and (c) photolithography method. (d)-(f) Schematic illustrations of lateral integrated photonics, including (d) inkjet printing, (e) layer-by-layer stacking and (f) capillary-bridge lithography.

OLES patterns (up to 4500 pixels per inch) through photolithography. Lin and his coworkers [268] introduced a photolithographic patterning approach for fabricating red, green, and blue perovskite films on a single substrate for multicolor display applications.

There are also some other methods to fabricate laterally integrated organic photonics. For example, Jie et al. [269] developed sequential crystallization to prepare well-aligned laterally stacked organic microbelt heterojunction arrays. Liao et al. [270] used o-BCB photoisomerization molecules to fabricate inseries organic heterostructures with high controllability and designability. By selectively exposing portions of organic microcrystals to light through a predesigned mask, partial photochromic transformations create heterostructures with distinct properties.

4.1.2 Vertical integrated organic photonics

Inkjet printing is a mask-free, low-cost, and scalable technique that enables precise spatial control over material depositon [271-273]. This process involves two key steps: the ejection of microdroplets and the subsequent assembly within the droplets. By sequentially introducing different inks, inkjet printing enables the fabrication of multicomponent microstructure arrays. Inkjet printing can be utilized in both lateral and vertical integrated photonics. For instance, full-color pixelated microspherical cap arrays were produced by sequentially printing red, green, and blue (RGB) emissive inks on a single substrate. These arrays, with uniform geometry, exhibited lasing under pulsed laser excitation due to laser dye incorporation [274]. Yan et al. [275] used an inkjet printing strategy to print orthogonal dye solutions step-by-step, generating precisely patterned core-shell heterostructure arrays. They achieved low-threshold dual-wavelength lasing in each single core-shell microstructure.

The dip-coating method is a versatile technique for fabricating organic semiconductor films and devices. This process involves immersing a substrate into a solution containing semiconductor materials and then withdrawing it at a controlled speed to form a thin, uniform layer on its surface. Hu et al. [276] developed a biphasic dip-coating method to fabricate p-n heterojunction composed of 1D/2D molecular crystals to produce significant negative photoresponse properties. They use the dip-coating method to fabricate the first-layer P-type 1D semiconductor arrays, and then transfer the freestanding N-type 2D molecular crystal from the surface of water to the as-prepared 1D semiconductor arrays, forming a high-quality P-N heterojunction via strong van der Waals interactions.

Wu et al. [277] established a facile sandwiched assembly system by utilizing a silicon pillar template with asymmetric wettability to control the nucleation and the unidirectional growth process of common solution-processable semiconducting materials, named the capillary-bridge lithography method. Then they utilized this method, combined with a two-step solution-processing strategy, successfully fabricating aligned two-component heterostructure arrays. Two semiconductor materials, MAPbBr3 and P3HT, were used to grow the acquired cross-stacked P3HT/MAPbBr3 heterostructure arrays. They further fabricated multi-component hierarchical heterostructure arrays with programmable geometries and tunable positional relationships using the sandwich structure assembly system. The fabrication of various hierarchical heterostructures, such as organic polymer/perovskite, organic polymer/nanoparticles, and nanoparticles/perovskite fabrication, was demonstrated using the hierarchical assembly strategy.

4.2 Organic photonic integrated circuits

PICs integrate essential photonic functions for optical communication and processing onto a single chip, offering advantages such as compact size, cost-effectiveness, reliability, and low power consumption [278]. As part of this innovative progress, the applications of organic materials in PICs have experienced rapid advancements in recent years.

Organics possess large thermo-optical (TO) coefficients and low thermal conductivity characteristics, which are essential for the development of low-power consumption thermo-optical switches (TOSs) [279-282] and modulators [283-285] for dynamic PICs. Chen et al. [286] developed a novel polymer TOS with a low polarization-dependent loss of 0.4 dB and a crosstalk of 30 dB. Moreover, a 1×576 switch is prepared by cascading the 1×24 switches, forming a record-low-loss TO waveguide lens (Figure 15(a)), offering a novel, alternative, and pragmatic approach for constructing large-scale optical switches that can find extensive applications in telecommunications, data communication, and optical computing. What's more, organics like polydimethylsiloxane (PDMS) and polystyrene (PS) with low Young's modulus usually show high photoelastic performance, indicating good candidates for ultrasonic detectors [287-289]. Li et al. [290] prepared a PS microring resonator with a PDMS substrate, realizing an axial resolution of 3.57 μm in mice brain imaging *in vivo* (Figure 15(b)). In addition, organics are also more suitable for hybrid integration with different active and passive photonics platforms due to their low processing temperature and simple device fabrication process [291-295]. Yue et al. [296] proposed a triple-layered optical interconnecting integrated chip, consisting of a 4×4 array waveguide grating-based wavelength-selective switching array with the wavelength-shifting sensitivity of 0.48 nm/°C, 4×4 multi-mode interference-cascaded channel-selective switching arrays with the average switch time of 280 μs and 3×3 direct-coupling interlayered switching arrays with the extinction ratio of 15.2 dB, based

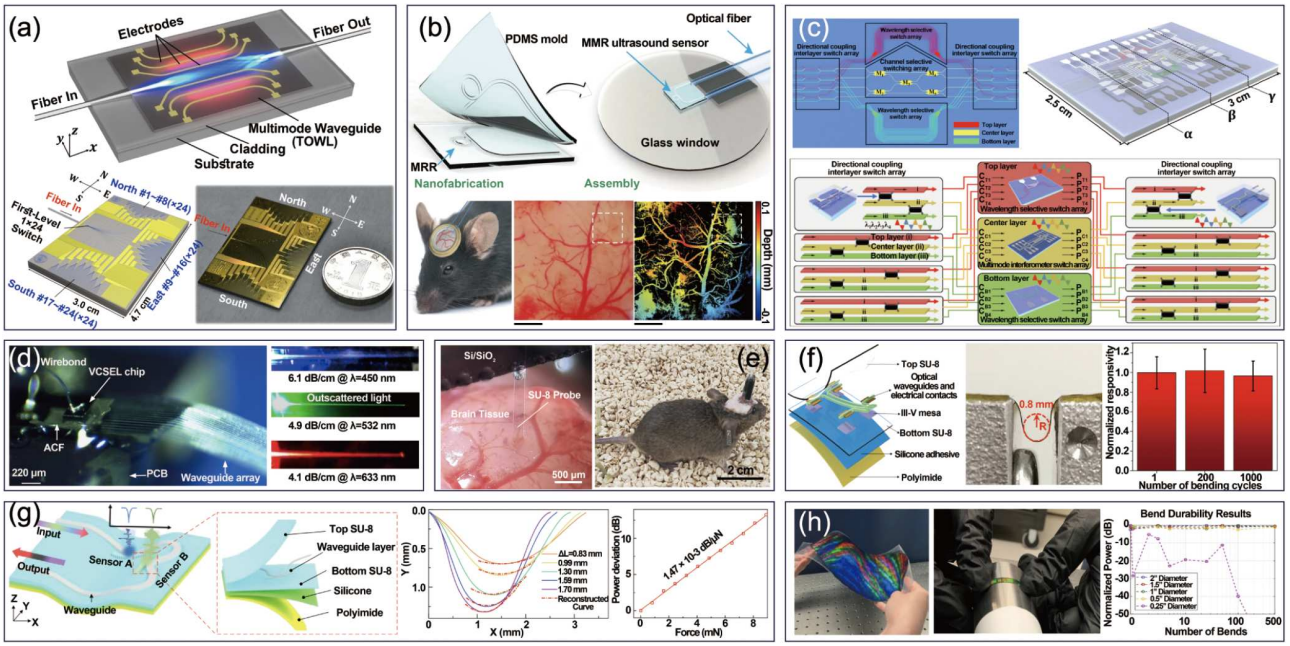

Figure 15 (Color online) (a) Polymer waveguide-integrated switch array. Reproduced with permission from ref. [286]. (b) PS MRR-based ultrasonic sensing for ultrasound imaging *in vivo*. Reproduced with permission from ref. [290]. (c) Triple-layered optical interconnecting integrated chips based on fluorinated epoxy. Reproduced with permission from ref. [296]. (d) Parylene C waveguide-integrated optogenetic probes. Reproduced with permission from ref. [298]. (e) Implantation-assistance-free flexible SU-8 waveguide probe for optogenetic stimulation. Reproduced with permission from ref. [299]. Copyright 2024 Elsevier. (f) Flexible waveguide-integrated detectors. Reproduced with permission from ref. [304]. (g) Flexible waveguide-integrated strain sensors. Reproduced with permission from ref. [301]. Copyright 2023 ACS. (h) Flexibility of 300 mm silicon nitride wafers. Reproduced with permission from ref. [306].

on fluorinated epoxy (Figure 15(c)). The multilayer stacked PIC is beneficial for high-speed and high-capacity photonic interconnecting systems. Meanwhile, taking advantage of the accessible preparation properties and intrinsic mechanical flexibility of polymer devices, organics continue to exhibit a diverse range of applications, particularly in flexible optogenetic probes [297]. Reddy et al. [298] demonstrated a flexible, visible waveguide array composed of Parylene C and PDMS (Figure 15(d)). However, deep probe implantation into brain tissue without assistance remains challenging due to its natural flexibility. To solve this problem, Chen et al. [299] developed a flexible polymer-waveguide optogenetic probe. The probe achieves a delicate balance between the inherent flexibility and rigidity of the polymer, and its meticulous geometric design facilitates precise, direct, and deep implantation without additional assistance, greatly reducing the difficulty of surgery and achieving the modulation of mouse motion speed (Figure 15(e)).

In recent years, introducing diverse inorganic optical materials in flexible substrates to construct high-index contrast (HIC) photonics has provided new ideas for functional and compact integrated photonic devices. And a series of functional device designs and fabrication methods [2,300], as well as their applications, including strain sensors [301-303], photodetectors [304] and switches [305] were developed, showing remarkable optoelectronic and mechanical performance. For example, Li et al. [304] developed the first flexible single-mode chalcogenide waveguide-integrated $In_{0.53}Ga_{0.47}As$ detector with a noise equivalent power as low as 0.02 pW $Hz^{1/2}$, a linear dynamic range over 70 dB and a 3 dB bandwidth of 1.4 GHz (Figure 15(f)). Luo et al. [301] proposed a waveguide-integrated flexible mechanical sensor using cascaded photonic crystal microcavities, which offers advanced multiplexing and achieves 110 μm resolution for 2D shape reconstruction. The sensor also enables quasi-distributed strain sensing and detects low force levels as small as 13.6 μN, demonstrating exceptional sensitivity (Figure 15(g)). Notaros et al. [306] developed a fabrication process for 300 mm silicon nitride wafer flexibility, showing no degradation in the propagation loss under the bending of a single chip 2,000 times to a bend diameter of 0.5 inches (Figure 15(h)). These results fully mark a substantial advancement over current state-of-the-art flexible waveguide integrated devices.

This overview highlights just a fraction of the progress in the field, yet it is sufficient to showcase the immense potential of flexible photonics across different platforms and underscores a range of potential applications in communication, sensing, imaging and neuroscience, etc.

4.3 Organic integrated nonlinear photonics

Integrated photonics is a system of light-controlling components combined into a single chip. Light is confined,

propagates and modulated in waveguides. Integrated nonlinear photonics provides transformative capabilities for controlling, enhancing and manipulating material nonlinearities in miniaturized on-chip platforms. Because of its potentially low cost and high compatibility with complementary metal oxide semiconductor (CMOS) industry, silicon-on-insulator (SOI) waveguide based integrated nonlinear photonics became a mainstream technology driven by advances in optical communications [307]. However, challenges remain due to the high waveguide loss, strong two-photon absorption, and the lack of second-order nonlinearities.

Driven by the exceptionally high second- and third-order optical nonlinearities of organic materials, the possible roles of organic materials in nonlinear optics and photonics have been extensively explored by organic material chemists and optical physicians for several decades. Early efforts had been focused on the understanding of how to optimize microscopic nonlinearities as a function of structure [308]. With the developments in silicon-organic hybrid (SOH, Figure 16 (a)) and plasmonic-organic hybrid (POH) waveguide geometries [232] , it became feasible to utilize chromophores with very large second-order polarizabilities for electro-optic switching [224,309-311], to realize large third-order polarizabilities for all-optical switching [312,313].

Over the past decade, a newly emerging integrated photonic structure based on ultralow-loss whispering gallery mode (WGM) microcavities has witnessed considerable progress in nonlinear photonics (Figure 16(b)-(d)) [314,315]. Different from straight optical waveguides, light-matter interaction can be dramatically enhanced in WGM microcavities, owing to the ultrahigh quality factor and small mode volume [314,316]. The integration of organic nonlinear materials into this type of WGM microcavities could be instrumental in the practical implementation of emerging nonlinear photonic applications such as quantum information processing, ultraprecise frequency metrology and spectroscopy [317].

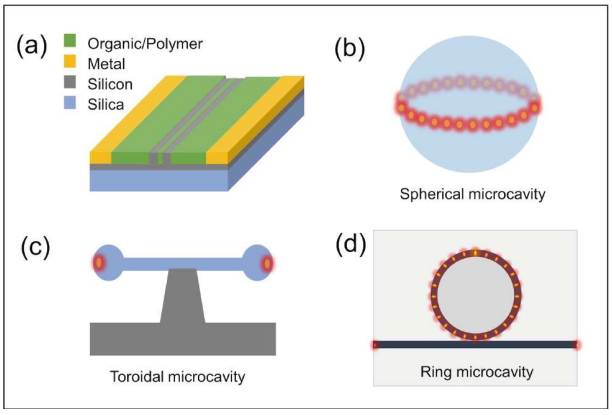

Figure 16 (Color online) Schematics of different waveguide structures for organic nonlinear photonics. (a) Conventional SOH waveguide geometry based on silicon slot waveguides. The optical field is guided by the straight silicon waveguides and interacts with the EO polymers in the slot. (b)-(d) newly emerging ultrahigh Q WGM microcavities: silica microsphere (a), silica microtoroid (b), and microring resonators made of other low loss materials such as silicon nitride or lithium niobate thin films (d). The optical fields are confined and dramatically enhanced in the ultrahigh Q WGM resonance modes. Organic NLO materials are grafted on the surface of the resonators to interact with the evanescent field of the circulating light.

Recently, Shen et al. [318,319] reported a type of organic-hybrid microcavity (OHM) device for organic materials for integrated nonlinear optics (Figure 17). The OHM devices utilized ultrahigh Q WGM microcavities to guide optical fields. An ultralow-loss, single layer of organic molecules was grated on the surface of the resonator via a chemical vapor deposition strategy. The organic NLO materials interact with the evanescent field of the circulating WGMs, enabling multiple nonlinear optical processes to be effectively excited with ultralow threshold power, by using low-power, continuous-wave pump lasers. This type of OHM device platforms features ultra-high quality factor of the WGM geometry and high surface optical nonlinearities of the organic materials simultaneously. This type of OHM photonic platforms opens up a new regime in organic nonlinear optics.

For example, the OHM device was first reported for optical parametric oscillation (OPO) frequency generation, which is an important NLO process for further generating optical frequency combs [318]. This process requires that the ultrahigh-Q cavity be fabricated from a material with a high third-order nonlinear coefficient and low dispersion. A single layer on organic NLO molecules with a very high third-order nonlinear coefficient was grafted on a silica spherical microcavity. The fabricated OHM device maintained ultrahigh Q values of above 1×10^7. It was demonstrated that the organic molecules not only help removing the parasitic secondary nonlinear effect, but also enabling the generation of low-threshold OPO in the OHM devices. The OPO efficiency was significantly enhanced by about three orders of magnitude, compared to a conventional silica microcavity.

Later on, the OHM devices were further investigated for low threshold third harmonic frequency, which is typically inefficiency to occur in conventional bare silica WMG microcavities due to the low third-order nonlinearity of silica [320]. By leveraging dynamic phase matching, the OHM silica devices were studied for third-harmonic frequency and sum-frequency generation. A record conversion efficiency of ~1680%/W^2 was achieved for third-harmonic generation, which is about four-order of magnitude higher compared to a conventional bare silica microcavity.

In addition to organic NLO molecules with extended π-electron conjugation, organic molecules without π-electron structures can also be of great interest for OHM nonlinear photonic devices. Shen et al. [321] used a simple organic

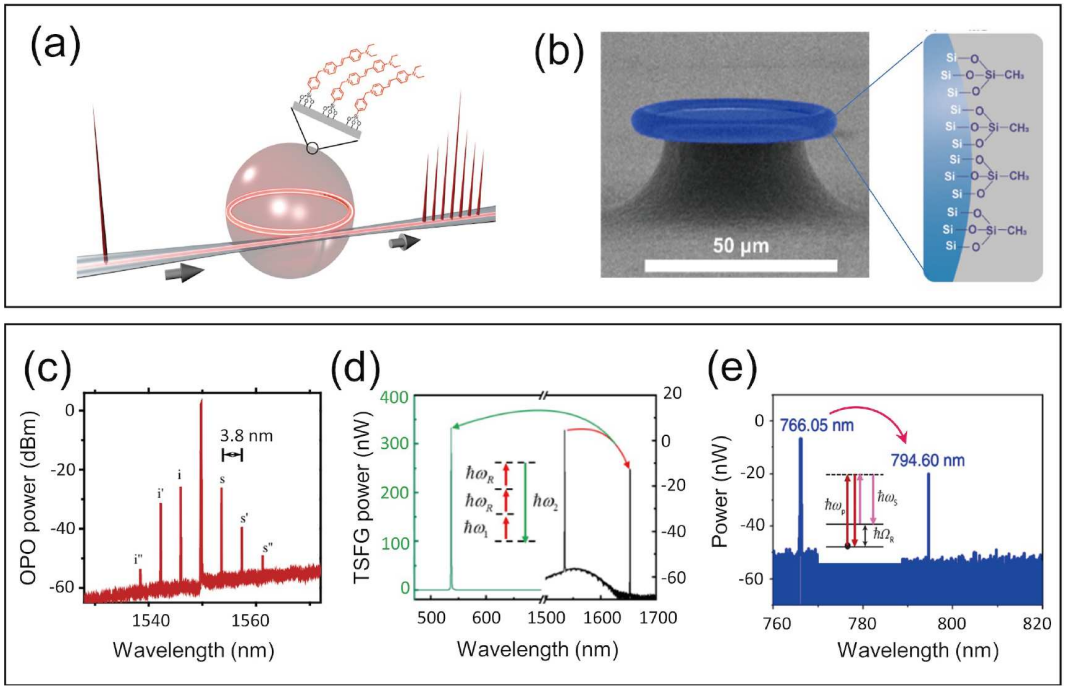

Figure 17 (Color online) (a) Schematic of an OHM device based on an ultrahigh Q silica microsphere for OPO frequency generation. A conjugated molecular layer on the surface is illustrated. (b) TEM image of an OHM device based on an ultrahigh Q silica microtorod on a silicon chip. (c)-(e) Output spectra of OPO frequency generation (c), third-harmonic generation frequency (d), and surface Raman lasing (e). (a) and (c) were reproduced from ref. [318]. (b) and (e) were reproduced from ref. [321]. (d) was reproduced with permission from ref. [320]. Copyright 2019 American Physical Society.

siloxane molecule to functionalize the surface of a toroidal optical microcavity on a silicon chip, with the aim of constructing a highly oriented Si-O-Si vibrational surface Raman mode. As a result of the selective interaction between the circulating polarized optical field of the WGM mode and the highly aligned surface Raman mode, a type of nonlinear optical process called surface stimulated Raman scattering was effectively excited in the OHM device. Moreover, it further resulted in the generation of surface Raman lasing behaviors in the OHM devices, with dramatically enhanced Raman lasing performance from ~5% to over ~40% efficiency compared with bulk silica devices.

Except for EO modulating, second-order optical nonlinearity is also of paramount importance to realize integrated frequency microcombs, quantum light generation, and frequency self-referencing [322]. Recently, it was reported that silica-based OHM photonic devices could be used for inducing strong second-order nonlinearity in photonic devices made of centrosymmetric material [323]. With an asymmetrically aligned monomolecular layer grafted on the surface of silica WGM microcavities, OHM devices with a strong symmetry-broken dipolar surface were fabricated. Under dual mode resonance matching conditions, the OHM devices were demonstrated to have significantly enhanced SHG efficiencies, owing to the monolayer molecules interacting with the optical evanescent field. The demonstrated strategy would open new opportunities for OHM devices in integrated second-order photonics.

5 Challenges and future perspectives

5.1 Intelligent material design based on machine learning

The photonic functionalities of organic materials are fundamentally governed by their excited-state processes, including radiative decay, intersystem crossing, exciton diffusion, and charge-transfer dynamics. These processes can be finely tuned through molecular structure design and intermolecular interaction engineering, such as donor-acceptor substitution, aggregation-induced emission (AIE), excimer formation, and exciton-phonon coupling. Importantly, when confined within micro/nanostructured architectures, these excited-state pathways can exhibit emergent behaviors due to altered dielectric environments, spatial constraints, and optical feedback mechanisms. Understanding and controlling these pathways at both the molecular and supramolecular levels is key to optimizing light-emitting efficiency, modulation speed, and spectral tunability in organic nanophotonic devices.

With the growing complexity of molecular design space, data-driven approaches—particularly those based on machine learning (ML) and high-throughput virtual screening—are emerging as powerful tools for accelerating the discovery

of high-performance photonic materials. By capturing structure-property relationships from large datasets, ML models can effectively predict key excited-state parameters (e.g., oscillator strength, exciton lifetime, singlet-triplet gaps) and guide inverse design strategies. The integration of intelligent algorithms with synthetic chemistry and photophysical modeling holds great promise for realizing next-generation organic materials with unprecedented optical properties tailored for specific nanophotonic applications.

5.2 Stability and lifetime of organic photonic devices

The stability and lifetime of organic photonic devices are critical factors influencing their practical applications and commercial viability. Organic photonic devices, including OLEDs, organic lasers, OPVs, and organic photodetectors, have garnered significant attention due to their flexibility, lightweight nature, and tunable optical properties. However, their stability and operational lifetime often lag behind their inorganic counterparts, posing challenges for widespread adoption. Typically, the device lifetime is typically measured in terms of the time taken for a device's performance to drop to 50% of its initial value, known as T50. Accelerated aging tests under controlled conditions (e.g., elevated temperatures or high humidity) are used to predict long-term stability.

The stability of organic photonic devices is mainly governed by the following two aspects, which are intrinsic material stability and device operation stability. On the one hand, organic materials are prone to degradation due to their molecular structure. Exposure to environmental factors such as oxygen, moisture, UV light, and heat can lead to chemical reactions, such as oxidation or hydrolysis, that degrade the active layers. For example, in OLEDs, the organic emissive layers may suffer from exciton-induced degradation during prolonged operation. On the other hand, organic devices are highly sensitive to environmental exposure. Inadequate encapsulation can lead to rapid degradation of device performance, making robust barrier layers essential for improving stability and lifetime.

To further boost the device stability, researchers in the field have proposed a material engineering strategy to develop more stable organic semiconductors, such as materials with higher glass transition temperatures or stronger molecular bonds, which can enhance intrinsic stability. The incorporation of cross-linked or polymeric materials can also improve mechanical and thermal robustness. Additionally, high-performance encapsulation technologies, such as thin-film encapsulation (TFE) or multilayer barrier coatings, are critical for protecting devices from environmental factors. These techniques involve alternating layers of organic and inorganic materials to create effective barriers against moisture and oxygen. Furthermore, replacing reactive metals with more stable alternatives, such as transparent conductive oxides (e.g., indium tin oxide) or carbon-based electrodes (e.g., graphene), can mitigate degradation. Introducing buffer layers or interlayers can protect the active materials from direct contact with electrodes. Lastly, lowering operational voltages and optimizing device driving conditions can reduce stress on the active materials, thereby prolonging device lifetime. Pulse driving or duty cycling is another approach to minimize continuous exposure to high current densities.

Overall, the stability and lifetime of organic photonic devices are improving with advancements in materials science, device engineering, and encapsulation technologies. While challenges remain, ongoing research is closing the gap between organic and inorganic photonic devices, paving the way for their broader adoption in flexible displays, wearable electronics.

5.3 Scalability and manufacturing

Currently, significant advancements have been made in the four aspects of organic photonics: optical generation, optical transportation, optical signal conversion and optical detection. However, it is difficult for a single organic structure to meet the multifunctional requirements of complex photonics. As the growth dimensions of organic crystals for different functional components are greatly different, such as organic microwires used as photodetectors and organic microcubes used as lasers, the reasonable integration of a single simple structure into the required complex heterostructures is still a bottleneck problem in synthesis. Fortunately, based on the lattice-matching principle and competitive intermolecular noncovalent interactions, a series of preparation methods for integrated organic photonics has been developed, including solution-based methods, photochromic approach, vapor deposition methods, doping approach, and crystallization-driven self-assembly of organic heterostructure. Nevertheless, despite significant achievements, a number of challenges remain that need to be further addressed. Therefore, we underscore the existing challenges and anticipate that tackling them will encourage ongoing research in this field.

(1) The techniques employed in the preparation of organic unconventional crystals are often unique, lacking standardized methodologies. Although there are many methods that can easily achieve the controlled self-assembly of integrated organic heterostructures during the growth process, the controlling space of the hierarchical organic micro-nano fine structure is very limited and the formation mechanism is still immature, which greatly limits its research and application in organic micro-nano optoelectronics. The significant differences in chemical and physical properties among various substances contribute to the diversity of crystallization mechanisms and conditions. Moreover, environmental factors such as temperature, pressure, and other elements play cru-

cial roles in the assembly mechanism. More efforts need to be devoted to understand the assembly kinetics and thermodynamics process of the complex conditions.

(2) Some prototype photonic devices have already been demonstrated in organic heterojunctions, but they are still far away from the ultimate goal of organic integrated photonics. Therefore, new fabrication methods for large-scale patterned devices and circuits are needed toward the realization of feasible organic photonic chips. Whereas promising methods have been developed for the synthesis of integrated organic heterostructures, there are no comparably robust and general methods that could precisely construct these heterostructures on a large scale. Considering that the present organic heterostructures integrated into the photonic components of PICs in a manner that is both effective and scalable remains a considerable challenge. It is critical for effectively controlling the nucleation and growth of crystals, thus realizing the ordered array growth of organic heterostructures. The currently reported patterning techniques are more or less dependent on the molecular structures and substrate properties. A universal process compatible with any organic molecule and substrate is still lacking. For example, the organic solvents involved in patterning procedures are not suitable for the flexible polymer substrates, which hinders their application in next generation wearable and stretchable devices.

5.4 Integration with conventional photonic technologies

In integrated photonics, high-confinement waveguides play a crucial role in harnessing the intrinsic nonlinearities of different material platforms. For high Q WGM microcavities, the nonlinearities of organic materials are typically several orders of magnitude higher than those of the counterpart inorganic materials, such as silica, silicon nitride and lithium niobate. However, organic materials also suffer from much higher optical losses, including both absorption and scattering loss. In particular, when organic layers are directly deposited—e.g., by spin-coating—onto micro- or nanoscale high-Q cavities, the resulting surface inhomogeneities and interface roughness often degrade the Q factor by two to three orders of magnitude. This dramatic reduction undermines the feasibility of efficient nonlinear optical processes. Therefore, precise control over the morphology, thickness, and uniformity of the organic layer at the micro- and nanoscale becomes critical to maintaining photonic performance.

Benefiting from the considerable advances in high-quality WGM microcavity photonics, integrated nonlinear photonics is entering into a new era. Beyond silicon, high-quality, low-cost, scalable silicon nitride and lithium niobate integrated materials platforms have shown promising potential in integrated nonlinear and quantum photonics. Nonetheless, these inorganic platforms inherently lack strong optical nonlinearities. The integration of organic NLO materials—especially through micro- and nanoscale patterning, hybrid lithography, or templated assembly—onto these platforms presents a compelling route to overcoming this limitation. Such micro/nano-engineered organic-inorganic hybrid photonic systems are expected to play a pivotal role in the development of next-generation compact, low-threshold, and functionally reconfigurable photonic devices.

This work was supported by the National Natural Science Foundation of China (Grant Nos. 22090023, 62175202, 52303236, and 62275152), the Beijing Natural Science Foundation (Grant No. 2252063), the Taishan Scholar Program of Shandong Province (Grant No. tsqn202306255), and the National Key Research and Development Program of China (Grant No. 2024YFB3612500).

Conflict of interest The authors declare that they have no conflict of interest.

1 H. Altug, S. H. Oh, S. A. Maier, and J. Homola, Nat. Nanotechnol. **17**, 5 (2022).
2 L. Li, H. Lin, S. Qiao, Y. Zou, S. Danto, K. Richardson, J. D. Musgraves, N. Lu, and J. Hu, Nat. Photonics **8**, 643 (2014).
3 Z. Yang, J. Xu, P. Wang, X. Zhuang, A. Pan, and L. Tong, Nano Lett. **11**, 5085 (2011).
4 L. N. Quan, J. Kang, C. Z. Ning, and P. Yang, Chem. Rev. **119**, 9153 (2019).
5 F. Qian, Y. Li, S. Gradečak, H. G. Park, Y. Dong, Y. Ding, Z. L. Wang, and C. M. Lieber, Nat. Mater. **7**, 701 (2008).
6 B. Piccione, C. H. Cho, L. K. van Vugt, and R. Agarwal, Nat. Nanotechnol. **7**, 640 (2012).
7 W. Zhang, and Y. S. Zhao, Chem. Commun. **52**, 8906 (2016).
8 J. Clark, and G. Lanzani, Nat. Photonics **4**, 438 (2010).
9 C. Zhang, Y. Yan, Y. S. Zhao, and J. Yao, Acc. Chem. Res. **47**, 3448 (2014).
10 W. Yao, Y. Yan, L. Xue, C. Zhang, G. Li, Q. Zheng, Y. S. Zhao, H. Jiang, and J. Yao, Angew. Chem. Int. Ed. **52**, 8713 (2013).
11 W. Zhang, J. Yao, and Y. S. Zhao, Acc. Chem. Res. **49**, 1691 (2016).
12 S. Kéna-Cohen, and S. R. Forrest, Nat. Photonics **4**, 371 (2010).
13 C. Zhang, C. L. Zou, Y. Yan, R. Hao, F. W. Sun, Z. F. Han, Y. S. Zhao, and J. Yao, J. Am. Chem. Soc. **133**, 7276 (2011).
14 Y. Yan, and Y. S. Zhao, Chem. Soc. Rev. **43**, 4325 (2014).
15 W. Zhang, Y. Yan, J. Gu, J. Yao, and Y. S. Zhao, Angew. Chem. Int. Ed. **54**, 7125 (2015).
16 H. Dong, Y. Wei, W. Zhang, C. Wei, C. Zhang, J. Yao, and Y. S. Zhao, J. Am. Chem. Soc. **138**, 1118 (2016).
17 Y. Yan, C. Zhang, J. Yao, and Y. S. Zhao, Adv. Mater. **25**, 3627 (2013).
18 C. Zhang, C. L. Zou, Y. Zhao, C. H. Dong, C. Wei, H. Wang, Y. Liu, G. C. Guo, J. Yao, and Y. S. Zhao, Sci. Adv. **1**, e1500257 (2015).
19 J. Z. Zhang, X. B. Xu, Y. Gong, Z. B. Wang, X. Z. Qi, X. J. Liu, Y. H. Yang, Z. H. Tian, J. Q. Wang, Y. L. Zhang, et al., Nat. Commun. **16**, 8213 (2025).
20 Q. Liao, Q. Li, and Z. Li, Adv. Mater. **37**, 2306617 (2025).
21 J. Poater, M. Duran, M. Solà, and B. Silvi, Chem. Rev. **105**, 3911 (2005).
22 R. M. Hochstrasser, Rev. Mod. Phys. **34**, 531 (1962).
23 M. D. Watson, A. Fechtenkötter, and K. Müllen, Chem. Rev. **101**, 1267 (2001).
24 Z. J. Lv, Q. Lv, T. Z. Feng, J. H. Jiang, and X. D. Wang, J. Am. Chem. Soc. **146**, 25755 (2024).
25 Y. Guo, L. Xu, H. Liu, Y. Li, C. Che, and Y. Li, Adv. Mater. **27**, 985 (2015).

26 M. Li, W. Yao, J. D. Chen, H. Y. Lu, Y. S. Zhao, and C. F. Chen, J. Mater. Chem. C **2**, 8373 (2014).
27 D. Meng, R. Zheng, Y. Zhao, E. Zhang, L. Dou, and Y. Yang, Adv. Mater. **34**, e2107330 (2022).
28 Y. Yu, X. Y. Xia, C. F. Xu, Z. J. Lv, X. D. Wang, and L. S. Liao, J. Am. Chem. Soc. **146**, 11845 (2024).
29 X. Y. Xia, Q. Lv, Y. Yu, Z. L. Che, X. D. Wang, L. S. Liao, and S. T. Lee, Sci. China Mater. **67**, 946 (2024).
30 L. Sun, Y. Wang, F. Yang, X. Zhang, and W. Hu, Adv. Mater. **31**, e1902328 (2019).
31 X. Wang, Z. Wang, X. Wang, F. Kang, Q. Gu, and Q. Zhang, Angew. Chem. Int. Ed. **63**, e202416181 (2024).
32 L. Sun, W. Zhu, X. Zhang, L. Li, H. Dong, and W. Hu, J. Am. Chem. Soc. **143**, 19243 (2021).
33 P. Li, C. Ji, M. Liu, K. Müllen, and M. Yin, Chem. Mater. **35**, 4564 (2023).
34 S. Liu, Y. Lin, and D. Yan, Sci. Bull. **67**, 2076 (2022).
35 Y. Yu, Z. Z. Li, J. J. Wu, G. Q. Wei, Y. C. Tao, M. L. Pan, X. D. Wang, and L. S. Liao, ACS Photonics **6**, 1798 (2019).
36 M. Zhuo, Y. Tao, X. Wang, Y. Wu, S. Chen, L. Liao, and L. Jiang, Angew. Chem. Int. Ed. **57**, 11300 (2018).
37 X. H. Ding, Y. Z. Chang, C. J. Ou, J. Y. Lin, L. H. Xie, and W. Huang, Natl. Sci. Rev. **7**, 1906 (2020).
38 M. Zhuo, Y. Yuan, Y. Su, S. Chen, Y. Chen, Z. Feng, Y. Qu, M. Li, Y. Li, B. Hu, et al., Adv. Mater. **34**, e2107169 (2022).
39 C. F. Xu, Y. P. Liu, Y. Yu, X. Y. Meng, H. Zong, Q. Lv, X. Y. Xia, X. D. Wang, and L. S. Liao, J. Phys. Chem. Lett. **14**, 3047 (2023).
40 Y. D. Zhao, J. Han, Y. Chen, Y. Su, Y. M. Cao, B. Wu, S. M. Yu, M. D. Li, Z. Wang, M. Zheng, et al., ACS Nano **16**, 15000 (2022).
41 Q. Lv, X. D. Wang, W. Y. Yang, K. L. Wang, C. F. Xu, M. Zheng, and L. S. Liao, CCS Chem. **5**, 423 (2023).
42 X. Fang, X. Yang, D. Li, B. Lu, and D. Yan, Cryst. Growth Des. **18**, 6470 (2018).
43 M. Rohullah, V. V. Pradeep, J. Ravi, A. V. Kumar, and R. Chandrasekar, Angew. Chem. Int. Ed. **61**, e202202114 (2022).
44 W. Zhu, R. Zheng, Y. Zhen, Z. Yu, H. Dong, H. Fu, Q. Shi, and W. Hu, J. Am. Chem. Soc. **137**, 11038 (2015).
45 M. P. Zhuo, J. J. Wu, X. D. Wang, Y. C. Tao, Y. Yuan, and L. S. Liao, Nat. Commun. **10**, 3839 (2019).
46 M. Zhuo, Y. Su, Y. Qu, S. Chen, G. He, Y. Yuan, H. Liu, Y. Tao, X. Wang, and L. Liao, Adv. Mater. **33**, 2102719 (2021).
47 E. M. Engler, B. A. Scott, S. Etemad, T. Penney, and V. V. Patel, J. Am. Chem. Soc. **99**, 5909 (1977).
48 Y. Su, Z. F. Yao, B. Wu, Y. D. Zhao, J. Y. Han, J. H. Sun, M. P. Zhuo, J. Z. Fan, Z. S. Wang, J. Pei, et al., Matter **5**, 1520 (2022).
49 Q. Lv, X. D. Wang, Y. Yu, M. P. Zhuo, M. Zheng, and L. S. Liao, Nat. Commun. **13**, 3099 (2022).
50 Y. Su, B. Wu, M. P. Zhuo, Q. Lv, J. H. Sun, Y. D. Zhao, M. Chen, Z. S. Wang, and X. D. Wang, Matter **7**, 569 (2024).
51 J. Yang, Y. Ma, Y. Zong, M. Sun, Y. Wang, R. Zhang, J. Feng, C. Wang, S. Zhuo, J. Zhou, et al., Small **20**, 2307129 (2024).
52 J. Zhang, S. Zhao, J. Jiang, Z. Lv, J. Luo, Y. Shi, Z. Lu, and X. Wang, Small **20**, 2400313 (2024).
53 Z. Qi, Y. Ma, and D. Yan, Aggregate **5**, e411 (2024).
54 S. Guan, G. Zhao, Y. Sun, Z. Tang, J. Pan, J. Wang, Z. Ji, and X. Wang, CrystEngComm **25**, 2655 (2023).
55 Y. Q. Sun, Y. L. Lei, X. H. Sun, S. T. Lee, and L. S. Liao, Chem. Mater. **27**, 1157 (2015).
56 H. Dong, S. Jiang, L. Jiang, Y. Liu, H. Li, W. Hu, E. Wang, S. Yan, Z. Wei, W. Xu, et al., J. Am. Chem. Soc. **131**, 17315 (2009).
57 H. Dong, X. Fu, J. Liu, Z. Wang, and W. Hu, Adv. Mater. **25**, 6158 (2013).
58 Y. Liu, H. Dong, S. Jiang, G. Zhao, Q. Shi, J. Tan, L. Jiang, W. Hu, and X. Zhan, Chem. Mater. **25**, 2649 (2013).
59 R. Liu, W. Yang, W. Xu, J. Deng, C. Ding, Y. Guo, L. Zheng, J. Sun, and M. Li, ACS Appl. Polym. Mater. **4**, 2233 (2022).
60 R. Grisorio, and G. P. Suranna, Polym. Chem. **6**, 7781 (2015).
61 T. Yokozawa, and Y. Ohta, Chem. Rev. **116**, 1950 (2016).
62 V. Senkovskyy, R. Tkachov, H. Komber, A. John, J. U. Sommer, and A. Kiriy, Macromolecules **45**, 7770 (2012).
63 Z. J. Bryan, and A. J. McNeil, Chem. Sci. **4**, 1620 (2013).
64 A. Yokoyama, and T. Yokozawa, Macromolecules **40**, 4093 (2007).
65 T. Lei, J. Y. Wang, and J. Pei, Chem. Mater. **26**, 594 (2013).
66 J. Mei, and Z. Bao, Chem. Mater. **26**, 604 (2013).
67 I. Osaka, and R. D. McCullough, Acc. Chem. Res. **41**, 1202 (2008).
68 A. Marrocchi, D. Lanari, A. Facchetti, and L. Vaccaro, Energy Environ. Sci. **5**, 8457 (2012).
69 M. T. Dang, L. Hirsch, G. Wantz, and J. D. Wuest, Chem. Rev. **113**, 3734 (2013).
70 S. Y. Son, J. H. Kim, E. Song, K. Choi, J. Lee, K. Cho, T. S. Kim, and T. Park, Macromolecules **51**, 2572 (2018).
71 S. Jin, I. Kim, J. A. Lim, H. Ahn, and E. Lee, Adv. Funct. Mater. **26**, 3226 (2016).
72 C. Meng, C. Liu, and S. Fan, Adv. Mater. **22**, 535 (2010).
73 C. Cho, K. L. Wallace, P. Tzeng, J. Hsu, C. Yu, and J. C. Grunlan, Adv. Energy Mater. **6**, 1502168 (2016).
74 Z. Zhang, G. Chen, H. Wang, and W. Zhai, J. Mater. Chem. C **3**, 1649 (2015).
75 L. Wang, C. Pan, Z. Chen, W. Zhou, C. Gao, and L. Wang, ACS Appl. Energy Mater. **1**, 5075 (2018).
76 B. Saparov, and D. B. Mitzi, Chem. Rev. **116**, 4558 (2016).
77 K. Leng, W. Fu, Y. Liu, M. Chhowalla, and K. P. Loh, Nat. Rev. Mater. **5**, 482 (2020).
78 B. R. Sutherland, and E. H. Sargent, Nat. Photonics **10**, 295 (2016).
79 M. D. Smith, B. A. Connor, and H. I. Karunadasa, Chem. Rev. **119**, 3104 (2019).
80 K. Wang, J. Y. Park, J. Y. Akriti, and L. Dou, Ecomat **3**, e12104 (2021).
81 K. Wang, J. H. Kim, J. Yang, X. Liu, Y. Dou, Y. Li, W. Tao, H. Dong, H. Zhu, K. Wu, et al., Sci. China Chem. **67**, 1776 (2024).
82 H. Dong, C. Zhang, X. Liu, J. Yao, and Y. S. Zhao, Chem. Soc. Rev. **49**, 951 (2020).
83 G. Xing, N. Mathews, S. S. Lim, N. Yantara, X. Liu, D. Sabba, M. Grätzel, S. Mhaisalkar, and T. C. Sum, Nat. Mater. **13**, 476 (2014).
84 H. Zhu, Y. Fu, F. Meng, X. Wu, Z. Gong, Q. Ding, M. V. Gustafsson, M. T. Trinh, S. Jin, and X. Y. Zhu, Nat. Mater. **14**, 636 (2015).
85 F. Deschler, M. Price, S. Pathak, L. E. Klintberg, D. D. Jarausch, R. Higler, S. Hüttner, T. Leijtens, S. D. Stranks, H. J. Snaith, et al., J. Phys. Chem. Lett. **5**, 1421 (2014).
86 X. K. Liu, W. Xu, S. Bai, Y. Jin, J. Wang, R. H. Friend, and F. Gao, Nat. Mater. **20**, 10 (2021).
87 M. Li, Y. Yang, Z. Kuang, C. Hao, S. Wang, F. Lu, Z. Liu, J. Liu, L. Zeng, Y. Cai, et al., Nature **630**, 631 (2024).
88 J. S. Kim, J. M. Heo, G. S. Park, S. J. Woo, C. Cho, H. J. Yun, D. H. Kim, J. Park, S. C. Lee, S. H. Park, et al., Nature **611**, 688 (2022).
89 H. D. Lee, S. J. Woo, S. Kim, J. Kim, H. Zhou, S. J. Han, K. Y. Jang, D. H. Kim, J. Park, S. Yoo, et al., Nat. Nanotechnol. **19**, 624 (2024).
90 D. Fu, J. Xin, Y. He, S. Wu, X. Zhang, X. Zhang, and J. Luo, Angew. Chem. Int. Ed. **60**, 20021 (2021).
91 P. Cheng, X. Jia, S. Chai, G. Li, M. Xin, J. Guan, X. Han, W. Han, S. Zeng, Y. Zheng, et al., Angew. Chem. Int. Ed. **63**, e202400644 (2024).
92 W. Zhang, L. Peng, J. Liu, A. Tang, J. Hu, J. Yao, and Y. S. Zhao, Adv. Mater. **28**, 4040 (2016).
93 X. Wu, H. Ji, X. Yan, and H. Zhong, Nat. Nanotechnol. **17**, 813 (2022).
94 T. H. Han, K. Y. Jang, Y. Dong, R. H. Friend, E. H. Sargent, and T. W. Lee, Nat. Rev. Mater. **7**, 757 (2022).
95 W. P. Lustig, S. Mukherjee, N. D. Rudd, A. V. Desai, J. Li, and S. K. Ghosh, Chem. Soc. Rev. **46**, 3242 (2017).
96 Y. Cui, J. Zhang, H. He, and G. Qian, Chem. Soc. Rev. **47**, 5740 (2018).
97 P. Li, Z. Zhou, Y. S. Zhao, and Y. Yan, Chem. Commun. **57**, 13678 (2021).

98 M. D. Allendorf, C. A. Bauer, R. K. Bhakta, and R. J. T. Houk, Chem. Soc. Rev. **38**, 1330 (2009).
99 B. Yan, Acc. Chem. Res. **50**, 2789 (2017).
100 M. Pan, Y. Zhu, K. Wu, L. Chen, Y. Hou, S. Yin, H. Wang, Y. Fan, and C. Su, Angew. Chem. Int. Ed. **56**, 14582 (2017).
101 X. Liu, K. Wang, Z. Chang, Y. Zhang, J. Xu, Y. S. Zhao, and X. Bu, Angew. Chem. Int. Ed. **58**, 13890 (2019).
102 Y. Yao, Z. Gao, Y. Lv, X. Lin, Y. Liu, Y. Du, F. Hu, and Y. S. Zhao, Angew. Chem. Int. Ed. **58**, 13803 (2019).
103 Z. Gao, B. Xu, T. Zhang, Z. Liu, W. Zhang, X. Sun, Y. Liu, X. Wang, Z. Wang, Y. Yan, et al., Angew. Chem. Int. Ed. **59**, 19060 (2020).
104 Z. Gao, S. Yang, B. Xu, T. Zhang, S. Chen, W. Zhang, X. Sun, Z. Wang, X. Wang, X. Meng, et al., Angew. Chem. Int. Ed. **60**, 24519 (2021).
105 R. Medishetty, J. K. Zaręba, D. Mayer, M. Samoć, and R. A. Fischer, Chem. Soc. Rev. **46**, 4976 (2017).
106 H. He, H. Li, Y. Cui, and G. Qian, Adv. Opt. Mater. **7**, 1900077 (2019).
107 Y. Lv, Z. Xiong, Z. Yao, Y. Yang, S. Xiang, Z. Zhang, and Y. S. Zhao, J. Am. Chem. Soc. **141**, 19959 (2019).
108 R. Medishetty, V. Nalla, L. Nemec, S. Henke, D. Mayer, H. Sun, K. Reuter, and R. A. Fischer, Adv. Mater. **29**, 1605637 (2017).
109 H. Tsai, S. Shrestha, R. A. Vilá, W. Huang, C. Liu, C. H. Hou, H. H. Huang, X. Wen, M. Li, G. Wiederrecht, et al., Nat. Photon. **15**, 843 (2021).
110 C. Zhang, B. Wang, W. Li, S. Huang, L. Kong, Z. Li, and L. Li, Nat. Commun. **8**, 1138 (2017).
111 J. Yu, Y. Cui, H. Xu, Y. Yang, Z. Wang, B. Chen, and G. Qian, Nat. Commun. **4**, 2719 (2013).
112 H. He, E. Ma, Y. Cui, J. Yu, Y. Yang, T. Song, C. D. Wu, X. Chen, B. Chen, and G. Qian, Nat. Commun. **7**, 11087 (2016).
113 Y. Liu, H. Dong, K. Wang, Z. Gao, C. Zhang, X. Liu, Y. S. Zhao, and F. Hu, ACS Appl. Mater. Interfaces **10**, 35455 (2018).
114 Z. Gao, B. Xu, Y. Fan, T. Zhang, S. Chen, S. Yang, W. Zhang, X. Sun, Y. Wei, Z. Wang, et al., Angew. Chem. Int. Ed. **60**, 6362 (2021).
115 J. Perego, C. X. Bezuidenhout, I. Villa, F. Cova, R. Crapanzano, I. Frank, F. Pagano, N. Kratochwill, E. Auffray, S. Bracco, et al., Nat. Commun. **13**, 3504 (2022).
116 V. W. W. Yam, V. K. M. Au, and S. Y. L. Leung, Chem. Rev. **115**, 7589 (2015).
117 M. J. Sun, Y. Liu, W. Zeng, Y. S. Zhao, Y. W. Zhong, and J. Yao, J. Am. Chem. Soc. **141**, 6157 (2019).
118 Y. Ma, J. Ma, P. Wang, J. Niu, J. Zhang, C. Duan, S. Chen, C. Han, and H. Xu, Sci. Adv. **10**, eadk3983 (2024).
119 S. F. Wang, B. K. Su, X. Q. Wang, Y. C. Wei, K. H. Kuo, C. H. Wang, S. H. Liu, L. S. Liao, W. Y. Hung, L. W. Fu, et al., Nat. Photon. **16**, 843 (2022).
120 X. Wang, B. Yin, L. Jiang, C. Yang, Y. Liu, G. Zou, S. Chen, and M. Zhu, Science **381**, 784 (2023).
121 M. J. Sun, Y. Liu, Y. Yan, R. Li, Q. Shi, Y. S. Zhao, Y. W. Zhong, and J. Yao, J. Am. Chem. Soc. **140**, 4269 (2018).
122 J. Zhao, T. Zhang, X. Y. Dong, M. E. Sun, C. Zhang, X. Li, Y. S. Zhao, and S. Q. Zang, J. Am. Chem. Soc. **141**, 15755 (2019).
123 L. C. C. Lee, and K. K. W. Lo, Chem. Rev. **124**, 8825 (2024).
124 Z. Liu, W. He, and Z. Guo, Chem. Soc. Rev. **42**, 1568 (2013).
125 D. L. Ma, V. P. Y. Ma, D. S. H. Chan, K. H. Leung, H. Z. He, and C. H. Leung, Coord. Chem. Rev. **256**, 3087 (2012).
126 C. C. Frazier, M. A. Harvey, M. P. Cockerham, H. M. Hand, E. A. Chauchard, and C. H. Lee, J. Phys. Chem. **90**, 5703 (2002).
127 H. Zhang, X. Jiang, Y. Zhang, K. Duanmu, C. Wu, Z. Lin, J. Xu, J. Yang, Z. Huang, M. G. Humphrey, et al., J. Am. Chem. Soc. **146**, 28329 (2024).
128 Q. Wang, J. Jin, Z. Wang, S. Ren, Q. Ye, Y. Dou, S. Liu, A. Morris, C. Slebodnick, and L. Quan, J. Am. Chem. Soc. **146**, 8971 (2024).
129 M. Hughes, M. Spring, and A. Podoleanu, Appl. Opt. **49**, 99 (2010).
130 C. Grivas, and M. Pollnau, Laser Photonics Rev. **6**, 419 (2012).
131 M. T. Hill, and M. C. Gather, Nat. Photonics **8**, 908 (2014).
132 A. J. C. Kuehne, and M. C. Gather, Chem. Rev. **116**, 12823 (2016).
133 H. H. Fang, J. Yang, J. Feng, T. Yamao, S. Hotta, and H. B. Sun, Laser Photonics Rev. **8**, 687 (2014).
134 J. J. Wu, X. D. Wang, and L. S. Liao, ACS Photonics **6**, 2590 (2019).
135 Y. Jiang, Y. Y. Liu, X. Liu, H. Lin, K. Gao, W. Y. Lai, and W. Huang, Chem. Soc. Rev. **49**, 5885 (2020).
136 R. Muñoz-Mármol, F. Gordillo, V. Bonal, J. M. Villalvilla, P. G. Boj, J. A. Quintana, A. M. Ross, G. M. Paternò, F. Scotognella, G. Lanzani, et al., Adv. Funct. Mater. **31**, 2105073 (2021).
137 J. V. Caspar, E. M. Kober, B. P. Sullivan, and T. J. Meyer, J. Am. Chem. Soc. **104**, 630 (2002).
138 D. F. P. Pile, Nat. Photon. **15**, 637 (2021).
139 P. P. Sorokin, and J. R. Lankard, IBM J. Res. Dev. **10**, 162 (1966).
140 B. H. Soffer, and B. B. McFarland, Appl. Phys. Lett. **10**, 266 (1967).
141 N. Karl, Phys. Stat. Sol. (a) **13**, 651 (1972).
142 O. S. Avanesjan, V. A. Benderskii, V. K. Brikenstein, V. L. Broude, L. I. Korshunov, A. G. Lavrushko, and I. I. Tartakovskii, Mol. Cryst. Liquid Cryst. **29**, 165 (1974).
143 D. Moses, Appl. Phys. Lett. **60**, 3215 (1992).
144 P. Yin, Q. Zhang, and J. M. Shreeve, Acc. Chem. Res. **49**, 4 (2016).
145 M. Mochizuki, X. Z. Yu, S. Seki, N. Kanazawa, W. Koshibae, J. Zang, M. Mostovoy, Y. Tokura, and N. Nagaosa, Nat. Mater. **13**, 241 (2014).
146 K. S. Daskalakis, S. A. Maier, R. Murray, and S. Kéna-Cohen, Nat. Mater. **13**, 271 (2014).
147 D. Venkatakrishnarao, E. A. Mamonov, T. V. Murzina, and R. Chandrasekar, Adv. Opt. Mater. **6**, 1800343 (2018).
148 G. Wei, X. Wang, and L. Liao, Laser Photonics Rev. **14**, 2000257 (2020).
149 D. O'Carroll, I. Lieberwirth, and G. Redmond, Nat. Nanotechnol. **2**, 180 (2007).
150 B. Corbett, and D. McDonald, Electron. Lett. **31**, 2181 (1995).
151 J. Wu, X. Wang, and L. Liao, Laser Photonics Rev. **16**, 2200366 (2022).
152 S. Han, W. Zhang, B. Qiu, H. Dong, W. Chen, M. Chu, Y. Liu, X. Yang, F. Hu, and Y. S. Zhao, Adv. Opt. Mater. **6**, 1701077 (2018).
153 H. H. Fang, Q. D. Chen, J. Yang, H. Xia, B. R. Gao, J. Feng, Y. G. Ma, and H. B. Sun, J. Phys. Chem. C **114**, 11958 (2010).
154 S. Kushida, D. Okada, F. Sasaki, Z. Lin, J. Huang, and Y. Yamamoto, Adv. Opt. Mater. **5**, 1700123 (2017).
155 C. Yan, Y. Liu, W. Yang, J. Wu, X. Wang, and L. Liao, Angew. Chem. Int. Ed. **61**, e202210422 (2022).
156 J. Wu, M. Zhuo, R. Lai, S. Zou, C. Yan, Y. Yuan, S. Yang, G. Wei, X. Wang, and L. Liao, Angew. Chem. Int. Ed. **60**, 9114 (2021).
157 D. Okada, T. Nakamura, D. Braam, T. D. Dao, S. Ishii, T. Nagao, A. Lorke, T. Nabeshima, and Y. Yamamoto, ACS Nano **10**, 7058 (2016).
158 T. Xu, M. J. Wei, H. Zhang, Y. Q. Zheng, G. Chen, and B. Wei, Appl. Phys. Lett. **107**, 123301 (2015).
159 Y. S. Zhao, A. Peng, H. Fu, Y. Ma, and J. Yao, Adv. Mater. **20**, 1661 (2008).
160 Z. L. Che, C. C. Yan, X. D. Wang, and L. S. Liao, Adv. Photon. **6**, 014001 (2024).
161 A. S. D. Sandanayaka, T. Matsushima, F. Bencheikh, S. Terakawa, W. J. Potscavage, C. Qin, T. Fujihara, K. Goushi, J. C. Ribierre, and C. Adachi, Appl. Phys. Express **12**, 061010 (2019).
162 K. Yoshida, J. Gong, A. L. Kanibolotsky, P. J. Skabara, G. A. Turnbull, and I. D. W. Samuel, Nature **621**, 746 (2023).
163 Z. L. Gong, X. Zhu, Z. Zhou, S. W. Zhang, D. Yang, B. Zhao, Y. P. Zhang, J. Deng, Y. Cheng, Y. X. Zheng, et al., Sci. China Chem. **64**, 2060 (2021).
164 Y. Deng, M. Wang, Y. Zhuang, S. Liu, W. Huang, and Q. Zhao, Light Sci. Appl. **10**, 76 (2021).
165 J. F. Chen, Q. X. Gao, H. Yao, B. Shi, Y. M. Zhang, T. B. Wei, and Q. Lin, Chem. Commun. **60**, 6728 (2024).
166 X. Yang, X. Gao, Y. X. Zheng, H. Kuang, C. F. Chen, M. Liu, P. Duan, and Z. Tang, CCS Chem. **5**, 2760 (2023).
167 S. Ren, Z. Liu, P. Li, H. Liu, M. Lu, K. Wang, J. Yao, H. Dong, Q.

Yang, and Y. S. Zhao, Angew. Chem. Int. Ed. **64**, e202415092 (2025).
168 M. Lu, P. Li, X. Dong, Z. Jiang, S. Ren, J. Yao, H. Dong, and Y. S. Zhao, Angew. Chem. Int. Ed. **63**, e202408619 (2024).
169 S. Ji, M. Zeng, X. Zhan, H. Liu, Y. Zhou, K. Wang, Y. Yan, J. Yao, and Y. S. Zhao, J. Am. Chem. Soc. **146**, 22583 (2024).
170 S. Ji, Y. Zhou, L. Xiong, X. Liu, T. Zhu, X. Zhan, Y. Yan, J. Yao, K. Wang, and Y. S. Zhao, J. Am. Chem. Soc. **147**, 16674 (2025).
171 D. Yang, and D. Ma, Adv. Opt. Mater. **7**, 1800522 (2018).
172 H. Ren, J. Chen, Y. Li, and J. Tang, Adv. Sci. **8**, 2002418 (2020).
173 Y. Yu, W. Wang, W. Li, G. Wang, Y. Wang, Z. Lu, S. Li, W. Zhao, Y. Li, T. Liu, et al., Front. Chem. **9**, 832028 (2022).
174 Q. Dang, L. Hu, L. Yuan, X. Miao, A. Huang, J. Su, J. Wang, Y. Zhou, X. Chen, Q. Li, et al., Angew. Chem. Int. Ed. **62**, e202312538 (2023).
175 J. H. Vella, L. Huang, N. Eedugurala, K. S. Mayer, T. N. Ng, and J. D. Azoulay, Sci. Adv. **7**, eabg2418 (2021).
176 Z. Xu, A. Chandresh, A. Mauri, M. Esmaeilpour, V. Monnier, F. Odobel, L. Heinke, W. Wenzel, M. Kozlowska, S. Diring, et al., Angew. Chem. Int. Ed. **63**, e202414526 (2024).
177 J. Wolansky, C. Hoffmann, M. Panhans, L. C. Winkler, F. Talnack, S. Hutsch, H. Zhang, A. Kirch, K. M. Yallum, H. Friedrich, et al., Adv. Mater. **36**, e2402834 (2024).
178 T. Yan, J. Ge, L. Su, X. Liu, and X. Fang, Nano Lett. **23**, 8295 (2023).
179 D. Periyanagounder, T. Wei, T. Li, C. Lin, T. P. Gonçalves, H. Fu, D. Tsai, J. Ke, H. Kuo, K. Huang, et al., Adv. Mater. **32**, e1904634 (2020).
180 Y. Zhang, Z. Qin, H. Gao, T. Wang, C. Gao, X. Zhang, W. Hu, and H. Dong, Adv. Mater. **36**, e2404309 (2024).
181 C. W. Tang, and S. A. VanSlyke, Appl. Phys. Lett. **51**, 913 (1987).
182 S. Banerjee, P. Singh, P. Purkayastha, and S. Kumar Ghosh, Chem. — An Asian J. **20**, e202401291 (2025).
183 M. A. Baldo, M. E. Thompson, and S. R. Forrest, Nature **403**, 750 (2000).
184 D. Zhang, L. Duan, C. Li, Y. Li, H. Li, D. Zhang, and Y. Qiu, Adv. Mater. **26**, 5050 (2014).
185 J. Zeng, S. Song, Y. Fu, X. Peng, B. Z. Tang, and Z. Zhao, Sci. Adv. **11**, eadt7899 (2025).
186 Q. Peng, A. Obolda, M. Zhang, and F. Li, Angew. Chem. Int. Ed. **54**, 7091 (2015).
187 S. R. Forrest, Nature **428**, 911 (2004).
188 H. Zhao, C. E. Arneson, D. Fan, and S. R. Forrest, Nature **626**, 300 (2024).
189 M. A. Baldo, D. F. O'Brien, Y. You, A. Shoustikov, S. Sibley, M. E. Thompson, and S. R. Forrest, Nature **395**, 151 (1998).
190 H. Uoyama, K. Goushi, K. Shizu, H. Nomura, and C. Adachi, Nature **492**, 234 (2012).
191 Y. Liu, C. Li, Z. Ren, S. Yan, and M. R. Bryce, Nat. Rev. Mater. **3**, 18020 (2018).
192 S. Diesing, L. Zhang, E. Zysman-Colman, and I. D. W. Samuel, Nature **627**, 747 (2024).
193 D. Park, S. Kang, C. H. Ryoo, B. H. Jhun, S. Jung, T. N. Le, M. C. Suh, J. Lee, M. E. Jun, C. Chu, et al., Nat. Commun. **14**, 5589 (2023).
194 X. C. Fan, K. Wang, Y. Z. Shi, Y. C. Cheng, Y. T. Lee, J. Yu, X. K. Chen, C. Adachi, and X. H. Zhang, Nat. Photon. **17**, 280 (2023).
195 X. Luo, S. Song, H. Ni, H. Ma, D. Yang, D. Ma, Y. Zheng, and J. Zuo, Angew. Chem. Int. Ed. **61**, e202209984 (2022).
196 T. Huang, Q. Wang, H. Zhang, Y. Xin, Y. Zhang, X. Chen, D. Zhang, and L. Duan, Nat. Mater. **23**, 1523 (2024).
197 D. Zhang, and L. Duan, Nat. Photonics **15**, 173 (2021).
198 S. O. Jeon, K. H. Lee, J. S. Kim, S. G. Ihn, Y. S. Chung, J. W. Kim, H. Lee, S. Kim, H. Choi, and J. Y. Lee, Nat. Photonics **15**, 208 (2021).
199 C. Y. Chan, M. Tanaka, Y. T. Lee, Y. W. Wong, H. Nakanotani, T. Hatakeyama, and C. Adachi, Nat. Photonics **15**, 203 (2021).
200 W. Han, J. Liu, C. Ran, Z. Huang, G. Gao, J. You, and Z. Bin, Angew. Chem. Int. Ed. **62**, e202312297 (2023).
201 T. Huang, Q. Wang, H. Zhang, Y. Zhang, G. Zhan, D. Zhang, and L. Duan, Nat. Photon. **18**, 516 (2024).
202 L. Wu, Z. Xin, D. Liu, D. Li, J. Zhang, Y. Zhou, S. Wu, T. Wang, S. Su, W. Li, et al., Adv. Mater. **37**, e2416224 (2025).
203 X. Ai, E. W. Evans, S. Dong, A. J. Gillett, H. Guo, Y. Chen, T. J. H. Hele, R. H. Friend, and F. Li, Nature **563**, 536 (2018).
204 M. Ito, S. Shirai, Y. Xie, T. Kushida, N. Ando, H. Soutome, K. J. Fujimoto, T. Yanai, K. Tabata, Y. Miyata, et al., Angew. Chem. Int. Ed. **61**, e202201965 (2022).
205 A. Abdurahman, T. J. H. Hele, Q. Gu, J. Zhang, Q. Peng, M. Zhang, R. H. Friend, F. Li, and E. W. Evans, Nat. Mater. **19**, 1224 (2020).
206 H. Cho, S. Gorgon, H. Hung, J. Huang, Y. Wu, F. Li, N. C. Greenham, E. W. Evans, and R. H. Friend, Adv. Mater. **35**, e2303666 (2023).
207 A. Mizuno, R. Matsuoka, T. Mibu, and T. Kusamoto, Chem. Rev. **124**, 1034 (2024).
208 Y. Fan, Z. Wang, B. Zhao, C. Zou, and D. Di, Matter **7**, 2738 (2024).
209 K. Wang, and Y. S. Zhao, Chem **7**, 3221 (2021).
210 G. Yu, J. Gao, J. C. Hummelen, F. Wudl, and A. J. Heeger, Science **270**, 1789 (1995).
211 V. D. Mihailetchi, L. J. A. Koster, J. C. Hummelen, and P. W. M. Blom, Phys. Rev. Lett. **93**, 216601 (2004).
212 J. Wang, Y. Xie, K. Chen, H. Wu, J. M. Hodgkiss, and X. Zhan, Nat Rev Phys **6**, 365 (2024).
213 J. Liu, S. Chen, D. Qian, B. Gautam, G. Yang, J. Zhao, J. Bergqvist, F. Zhang, W. Ma, H. Ade, et al., Nat Energy **1**, 16089 (2016).
214 D. Qian, Z. Zheng, H. Yao, W. Tress, T. R. Hopper, S. Chen, S. Li, J. Liu, S. Chen, J. Zhang, et al., Nat. Mater. **17**, 703 (2018).
215 Y. Jiang, S. Sun, R. Xu, F. Liu, X. Miao, G. Ran, K. Liu, Y. Yi, W. Zhang, and X. Zhu, Nat Energy **9**, 975 (2024).
216 Z. Zheng, J. Wang, P. Bi, J. Ren, Y. Wang, Y. Yang, X. Liu, S. Zhang, and J. Hou, Joule **6**, 171 (2022).
217 L. Xu, S. Li, W. Zhao, Y. Xiong, J. Yu, J. Qin, G. Wang, R. Zhang, T. Zhang, Z. Mu, et al., Adv. Mater. **36**, e2403476 (2024).
218 L. Zhu, M. Zhang, G. Zhou, Z. Wang, W. Zhong, J. Zhuang, Z. Zhou, X. Gao, L. Kan, B. Hao, et al., Joule **8**, 3153 (2024).
219 U. Koch, C. Uhl, H. Hettrich, Y. Fedoryshyn, C. Hoessbacher, W. Heni, B. Baeuerle, B. I. Bitachon, A. Josten, M. Ayata, et al., Nat. Electron. **3**, 338 (2020).
220 W. Zhang, M. Ebert, K. Li, B. Chen, X. Yan, H. Du, M. Banakar, D. T. Tran, C. G. Littlejohns, A. Scofield, et al., Nat. Photon. **17**, 273 (2023).
221 H. Feng, T. Ge, X. Guo, B. Wang, Y. Zhang, Z. Chen, S. Zhu, K. Zhang, W. Sun, C. Huang, et al., Nature **627**, 80 (2024).
222 R. Ding, T. Baehr-Jones, Y. Liu, R. Bojko, J. Witzens, S. Huang, J. Luo, S. Benight, P. Sullivan, J. M. Fedeli, et al., Opt. Express **18**, 15618 (2010).
223 I. Taghavi, M. Moridsadat, A. Tofini, S. Raza, N. A. F. Jaeger, L. Chrostowski, B. J. Shastri, and S. Shekhar, Nanophotonics **11**, 3855 (2022).
224 G. W. Lu, J. Hong, F. Qiu, A. M. Spring, T. Kashino, J. Oshima, M. Ozawa, H. Nawata, and S. Yokoyama, Nat. Commun. **11**, 4224 (2020).
225 M. Thomaschewski, and S. I. Bozhevolnyi, Appl. Phys. Rev. **9**, 021311 (2022).
226 W. Heni, C. Haffner, D. L. Elder, A. F. Tillack, Y. Fedoryshyn, R. Cottier, Y. Salamin, C. Hoessbacher, U. Koch, B. Cheng, et al., Opt. Express **25**, 2627 (2017).
227 J. Wu, Z. Li, J. Luo, and A. K. Y. Jen, J. Mater. Chem. C **8**, 15009 (2020).
228 H. Xu, D. L. Elder, L. E. Johnson, W. Heni, Y. de Coene, E. De Leo, M. Destraz, N. Meier, W. Vander Ghinst, S. R. Hammond, et al., Mater. Horiz. **9**, 261 (2022).
229 M. Xu, M. He, H. Zhang, J. Jian, Y. Pan, X. Liu, L. Chen, X. Meng, H. Chen, Z. Li, et al., Nat. Commun. **11**, 3911 (2020).
230 H. Xu, F. Liu, D. L. Elder, L. E. Johnson, Y. de Coene, K. Clays, B.

H. Robinson, and L. R. Dalton, Chem. Mater. **32**, 1408 (2020).
231 Y. Wang, T. Liu, J. Liu, C. Li, Z. Chen, and S. Bo, J. Semicond. **43**, 101301 (2022).
232 W. Heni, Y. Kutuvantavida, C. Haffner, H. Zwickel, C. Kieninger, S. Wolf, M. Lauermann, Y. Fedoryshyn, A. F. Tillack, L. E. Johnson, et al., ACS Photonics **4**, 1576 (2017).
233 Y. Gao, G. Walters, Y. Qin, B. Chen, Y. Min, A. Seifitokaldani, B. Sun, P. Todorovic, M. I. Saidaminov, A. Lough, et al., Adv. Mater. **31**, e1808336 (2019).
234 M. Li, S. Huang, X. H. Zhou, Y. Zang, J. Wu, Z. Cui, J. Luo, and A. K. Y. Jen, J. Mater. Chem. C **3**, 6737 (2015).
235 Y. Salamin, B. Baeuerle, W. Heni, F. C. Abrecht, A. Josten, Y. Fedoryshyn, C. Haffner, R. Bonjour, T. Watanabe, M. Burla, et al., Nat. Photonics **12**, 749 (2018).
236 X. Sun, H. Yu, N. Deng, D. Ban, G. Liu, and F. Qiu, Opt. Express **29**, 25543 (2021).
237 R. Song, H. C. Song, W. H. Steier, and C. H. Cox, IEEE J. Quantum Electron. **43**, 633 (2007).
238 Y. Shi, C. Zhang, H. Zhang, J. H. Bechtel, L. R. Dalton, B. H. Robinson, and W. H. Steier, Science **288**, 119 (2000).
239 F. Qiu, A. M. Spring, J. Hong, H. Miura, T. Kashino, T. Kikuchi, M. Ozawa, H. Nawata, K. Odoi, and S. Yokoyama, Laser Photonics Rev. **11**, 1700061 (2017).
240 B. Bortnik, Y. C. Hung, H. Tazawa, B. J. Seo, J. Luo, A. K. Y. Jen, W. H. Steier, and H. R. Fetterman, IEEE J. Quantum Electron. **13**, 104 (2007).
241 S. Koeber, R. Palmer, M. Lauermann, W. Heni, D. L. Elder, D. Korn, M. Woessner, L. Alloatti, S. Koenig, P. C. Schindler, et al., Light Sci. Appl. **4**, e255 (2015).
242 L. Alloatti, R. Palmer, S. Diebold, K. P. Pahl, B. Chen, R. Dinu, M. Fournier, J. M. Fedeli, T. Zwick, W. Freude, et al., Light Sci. Appl. **3**, e173 (2014).
243 C. Kieninger, Y. Kutuvantavida, D. L. Elder, S. Wolf, H. Zwickel, M. Blaicher, J. N. Kemal, M. Lauermann, S. Randel, W. Freude, et al., Optica **5**, 739 (2018).
244 A. Melikyan, L. Alloatti, A. Muslija, D. Hillerkuss, P. C. Schindler, J. Li, R. Palmer, D. Korn, S. Muehlbrandt, D. Van Thourhout, et al., Nat. Photonics **8**, 229 (2014).
245 W. Heni, Y. Fedoryshyn, B. Baeuerle, A. Josten, C. B. Hoessbacher, A. Messner, C. Haffner, T. Watanabe, Y. Salamin, U. Koch, et al., Nat. Commun. **10**, 1694 (2019).
246 M. Burla, C. Hoessbacher, W. Heni, C. Haffner, Y. Fedoryshyn, D. Werner, T. Watanabe, H. Massler, D. L. Elder, L. R. Dalton, et al., APL Photonics **4**, 056106 (2019).
247 B. Vukovic, D. Moor, Y. Fedoryshyn, M. Baumann, T. Blatter, D. Chelladurai, M. Eleraky, H. Wang, and J. Leuthold, in *Microwave resonant plasmonic modulator for sub-THz receivers*: *Proceedings of the 2024 Conference on Lasers and Electro-Optics (CLEO)* (Optica Publishing Group, Charlotte, 2024).
248 M. Eppenberger, A. Messner, B. I. Bitachon, W. Heni, T. Blatter, P. Habegger, M. Destraz, E. De Leo, N. Meier, N. Del Medico, et al., Nat. Photon. **17**, 360 (2023).
249 C. Koos, J. Leuthold, W. Freude, M. Kohl, L. Dalton, W. Bogaerts, A. L. Giesecke, M. Lauermann, A. Melikyan, S. Koeber, et al., J. Lightwave Technol. **34**, 256 (2016).
250 M. Sun, C. Zheng, Y. Gao, A. Johnston, A. M. Najarian, P. Wang, O. Voznyy, S. Hoogland, and E. H. Sargent, Adv. Mater. **33**, e2006368 (2021).
251 J. Pfeifle, L. Alloatti, W. Freude, J. Leuthold, and C. Koos, Opt. Express **20**, 15359 (2012).
252 Y. Xing, T. Ako, J. P. George, D. Korn, H. Yu, P. Verheyen, M. Pantouvaki, G. Lepage, P. Absil, A. Ruocco, et al., IEEE Photon. Technol. Lett. **27**, 1269 (2015).
253 L.Y. Chiang, C.T. Wang, S. Pappert, and P.K.L.Yu, in *Efficient silicon photonic waveguide switches for chip-scale beam steering applications: Proceedings of the 5th IEEE Electron Devices Technology & Manufacturing Conference (EDTM)*. Chengdu, China, 8 April-11 April 2021 (New York, IEEE, 2021).
254 J. Jian, R. Liu, Y. Ye, J. Wu, Q. Deng, M. Wei, Y. Tang, R. Tang, B. Sun, H. Ma, et al., Adv. Opt. Mater. **12**, 2400281 (2024).
255 Y. Hou, Z. Gao, Y. S. Zhao, and Y. Yan, Org. Chem. Front. **7**, 2776 (2020).
256 X. Zhang, Y. Xiao, L. He, and Y. Zhang, J. Org. Chem. **79**, 6315 (2014).
257 H. Lee, J. Kim, H. Kim, J. Kim, and S. Kwon, Nat. Mater. **9**, 745 (2010).
258 J. Lee, P. W. Bisso, R. L. Srinivas, J. J. Kim, A. J. Swiston, and P. S. Doyle, Nat. Mater. **13**, 524 (2014).
259 Z. Gao, C. Wei, Y. Yan, W. Zhang, H. Dong, J. Zhao, J. Yi, C. Zhang, Y. J. Li, and Y. S. Zhao, Adv. Mater. **29**, 1701558 (2017).
260 X. Feng, R. Lin, S. Yang, Y. Xu, T. Zhang, S. Chen, Y. Ji, Z. Wang, S. Chen, C. Zhu, et al., Angew. Chem. Int. Ed. **62**, e202310263 (2023).
261 C. Zhang, Y. Yan, Y. Jing, Q. Shi, Y. S. Zhao, and J. Yao, Adv. Mater. **24**, 1703 (2012).
262 S. Yang, X. Feng, B. Xu, R. Lin, Y. Xu, S. Chen, Z. Wang, X. Wang, X. Meng, and Z. Gao, ACS Nano **17**, 6341 (2023).
263 Y. Zhang, H. Dong, Q. Tang, S. Ferdous, F. Liu, S. C. B. Mannsfeld, W. Hu, and A. L. Briseno, J. Am. Chem. Soc. **132**, 11580 (2010).
264 M. Choi, S. R. Bae, L. Hu, A. T. Hoang, S. Y. Kim, and J. H. Ahn, Sci. Adv. **6**, eabb5898 (2020).
265 Q. Lv, X. D. Wang, Y. Yu, C. F. Xu, Y. J. Yu, X. Y. Xia, M. Zheng, and L. S. Liao, Nat. Chem. **16**, 201 (2024).
266 Y. Choi, H. Shin, J. Son, C. Park, K. W. Park, J. K. Lee, and B. Jung, Micromachines **11**, 650 (2020).
267 H. Kweon, K. Y. Choi, H. W. Park, R. Lee, U. Jeong, M. J. Kim, H. Hong, B. Ha, S. Lee, J. Y. Kwon, et al., Nat. Commun. **13**, 6775 (2022).
268 C. Zou, C. Chang, D. Sun, K. F. Böhringer, and L. Y. Lin, Nano Lett. **20**, 3710 (2020).
269 X. Zhang, J. Mao, W. Deng, X. Xu, L. Huang, X. Zhang, S. Lee, and J. Jie, Adv. Mater. **30**, 1800187 (2018).
270 Z. Li, J. Wu, X. Wang, K. Wang, S. Zhang, W. Xie, and L. Liao, Adv. Opt. Mater. **7**, 1900373 (2019).
271 J. Zhao, Y. Yan, Z. Gao, Y. Du, H. Dong, J. Yao, and Y. S. Zhao, Nat. Commun. **10**, 870 (2019).
272 J. Wang, D. Li, L. Mu, M. Li, Y. Luo, B. Zhang, C. Mai, B. Guo, L. Lan, J. Wang, et al., ACS Appl. Mater. Interfaces **13**, 41773 (2021).
273 Y. Liu, F. Li, L. Qiu, K. Yang, Q. Li, X. Zheng, H. Hu, T. Guo, C. Wu, and T. W. Kim, ACS Nano **13**, 2042 (2019).
274 M. Zhu, Y. Duan, N. Liu, H. Li, J. Li, P. Du, Z. Tan, G. Niu, L. Gao, Y. A. Huang, et al., Adv. Funct. Mater. **29**, 1903294 (2019).
275 Z. Zhou, J. Zhao, Y. Du, K. Wang, J. Liang, Y. Yan, and Y. S. Zhao, Angew. Chem. Int. Ed. **59**, 11814 (2020).
276 X. Zhu, Y. Yan, L. Sun, Y. Ren, Y. Zhang, Y. Liu, X. Zhang, R. Li, H. Chen, J. Wu, et al., Adv. Mater. **34**, e2201364 (2022).
277 X. Fan, B. Zhang, J. Zhao, Y. Zhao, M. Yuan, Y. Geng, K. He, H. Li, J. Feng, Y. Fu, et al., ACS Mater. Lett. **4**, 770 (2022).
278 Y. Su, Y. He, X. Guo, W. Xie, X. Ji, H. Wang, X. Cai, L. Tong, and S. Yu, ACS Photonics **10**, 2020 (2023).
279 S. Sun, Q. Yu, Y. Che, T. Lian, Y. Xie, D. Zhang, and X. Wang, Photon. Res. **12**, 423 (2024).
280 B. Lin, X. Wang, J. Lv, Y. Cao, Y. Yang, Y. Zhang, A. Zhang, Y. Yi, F. Wang, and D. Zhang, Opt. Lett. **45**, 4448 (2020).
281 C. Chen, X. Niu, C. Han, Z. Shi, X. Wang, X. Sun, F. Wang, Z. Cui, and D. Zhang, Opt. Express **22**, 10716 (2014).
282 J. Dong, K. S. Chiang, and W. Jin, J. Lightwave Technol. **33**, 4580 (2015).
283 Z. Chen, M. Wei, Y. Luo, J. Jian, Y. Ye, Y. Yin, C. Sun, C. Zhong, K. Si, D. Zhang, et al., Opt. Mater. Express **12**, 4061 (2022).
284 J. Lv, Y. Yang, B. Lin, Y. Cao, Y. Zhang, S. Li, Y. Yi, F. Wang, and D. Zhang, Opt. Lett. **44**, 4606 (2019).
285 S. Sun, Y. Che, Y. Xie, Q. Yu, F. Wang, X. Wang, and D. Zhang, Opt. Lett. **48**, 5336 (2023).
286 T. Chen, Z. Dang, Z. Deng, S. Ke, Z. Ding, and Z. Zhang, PhotoniX

5, 14 (2024).
287 Y. Hazan, A. Levi, M. Nagli, and A. Rosenthal, Nat. Commun. **13**, 1488 (2022).
288 M. Nagli, R. Moisseev, N. Suleymanov, E. Kaminski, Y. Hazan, G. Gelbert, I. Goykhman, and A. Rosenthal, Photoacoustics **32**, 100527 (2023).
289 Z. Ding, J. Sun, C. Li, and Y. Shi, J. Lightwave Technol. **41**, 1906 (2023).
290 H. Li, B. Dong, X. Zhang, X. Shu, X. Chen, R. Hai, D. A. Czaplewski, H. F. Zhang, and C. Sun, Nat. Commun. **10**, 4277 (2019).
291 R. Yi, X. Zhang, F. Zhang, L. Gu, Q. Zhang, L. Fang, J. Zhao, L. Fu, H. H. Tan, C. Jagadish, et al., Nano Lett. **22**, 9920 (2022).
292 C. Wang, D. Zhang, J. Yue, X. Zhang, H. Lin, X. Sun, A. Cui, T. Zhang, C. Chen, and T. Fei, Nat. Commun. **14**, 4578 (2023).
293 M. Weigel, M. Kleinert, M. Kresse, D. de Felipe, H. Conradi, J. Reck, K. Mihov, T. Qian, C. Zawadzki, A. Scheu, et al., J. Lightwave Technol. **42**, 1511 (2024).
294 A. Raptakis, L. Gounaridis, M. Weigel, M. Kleinert, M. Georgiopoulos, E. Mylonas, P. Groumas, C. Tsokos, N. Keil, H. Avramopoulos, et al., J. Lightwave Technol. **39**, 6509 (2021).
295 Y. Cao, B. Lin, Y. Sun, Y. Yi, Y. Liu, J. Zheng, F. Wang, and D. Zhang, Sci. Rep. **8**, 13682 (2018).
296 J. Yue, X. Sun, C. Wang, S. Zhang, L. Han, J. Wang, Z. Cui, Z. Shi, D. Zhang, and C. Chen, Opt. Express **31**, 19415 (2023).
297 L. Rudmann, D. Scholz, M. T. Alt, A. Dieter, E. Fiedler, T. Moser, and T. Stieglitz, Adv. Health. Mater. **13**, 2304513 (2024).
298 J. W. Reddy, M. Lassiter, and M. Chamanzar, Microsyst. Nanoeng. **6**, 85 (2020).
299 Z. Chen, X. Li, Y. Tang, Z. Huang, J. Huang, H. Liu, Y. Weng, Y. Zhu, J. Zhao, R. Tang, et al., Cell Rep. Phys. Sci. **5**, 102217 (2024).
300 Z. Chen, Y. Shi, M. Wei, Y. Luo, H. Ma, R. Tang, Y. Weng, H. Dai, C. Zhong, C. Sun, et al., Adv. Opt. Mater. **11**, 2202824 (2023).
301 Y. Luo, C. Sun, M. Wei, H. Ma, Y. Wu, Z. Chen, H. Dai, J. Jian, B. Sun, C. Zhong, et al., Nano Lett. **23**, 8898 (2023).
302 L. Li, H. Lin, S. Qiao, Y. Z. Huang, J. Y. Li, J. Michon, T. Gu, C. Alosno-Ramos, L. Vivien, A. Yadav, et al., Light Sci. Appl. **7**, 17138 (2018).
303 J. Michon, S. Geiger, L. Li, C. Goncalves, H. Lin, K. Richardson, X. Jia, and J. Hu, Photon. Res. **8**, 194 (2020).
304 L. Li, H. Lin, Y. Huang, R. J. Shiue, A. Yadav, J. Li, J. Michon, D. Englund, K. Richardson, T. Gu, et al., Optica **5**, 44 (2018).
305 Z. Chen, M. Wei, B. Sun, Y. Weng, J. Jian, C. Zhong, C. Sun, K. Si, W. Gong, H. Lin, et al., Opt. Lett. **48**, 3239 (2023).
306 M. Notaros, T. Dyer, A. Garcia Coleto, A. Hattori, K. Fealey, S. Kruger, and J. Notaros, Sci. Rep. **14**, 10623 (2024).
307 J. Leuthold, C. Koos, and W. Freude, Nat. Photonics **4**, 535 (2010).
308 L. R. Dalton, P. A. Sullivan, and D. H. Bale, Chem. Rev. **110**, 25 (2010).
309 F. Ullah, N. Deng, and F. Qiu, PhotoniX **2**, 13 (2021).
310 I. C. Benea-Chelmus, M. L. Meretska, D. L. Elder, M. Tamagnone, L. R. Dalton, and F. Capasso, Nat. Commun. **12**, 5928 (2021).
311 H. Xu, D. L. Elder, L. E. Johnson, Y. de Coene, S. R. Hammond, W. Vander Ghinst, K. Clays, L. R. Dalton, and B. H. Robinson, Adv. Mater. **33**, e2104174 (2021).
312 C. Koos, P. Vorreau, T. Vallaitis, P. Dumon, W. Bogaerts, R. Baets, B. Esembeson, I. Biaggio, T. Michinobu, F. Diederich, et al., Nat. Photonics **3**, 216 (2009).
313 X. Hu, P. Jiang, C. Ding, H. Yang, and Q. Gong, Nat. Photonics **2**, 185 (2008).
314 K. J. Vahala, Nature **424**, 839 (2003).
315 J. Liu, F. Bo, L. Chang, C. H. Dong, X. Ou, B. Regan, X. Shen, Q. Song, B. Yao, W. Zhang, et al., Sci. China-Phys. Mech. Astron. **65**, 104201 (2022).
316 S. Feng, T. Lei, H. Chen, H. Cai, X. Luo, and A. W. Poon, Laser & Photonics Rev. **6**, 145 (2012).
317 A. Dutt, A. Mohanty, A. L. Gaeta, and M. Lipson, Nat. Rev. Mater. **9**, 321 (2024).
318 X. Shen, R. C. Beltran, V. M. Diep, S. Soltani, and A. M. Armani, Sci. Adv. **4**, eaao4507 (2018).
319 D. Chen, A. Kovach, X. Shen, S. Poust, and A. M. Armani, ACS Photonics **4**, 2376 (2017).
320 J. Chen, X. Shen, S. J. Tang, Q. T. Cao, Q. Gong, and Y. F. Xiao, Phys. Rev. Lett. **123**, 173902 (2019).
321 X. Shen, H. Choi, D. Chen, W. Zhao, and A. M. Armani, Nat. Photonics **14**, 95 (2020).
322 P. Liu, H. Wen, L. Ren, L. Shi, and X. Zhang, Front. Optoelectron. **16**, 18 (2023).
323 R. Wang, Y. Dai, J. Cheng, R. Wang, and X. Shen, Optica **12**, 769 (2025).